# Revisiting the East Asian summer monsoon structure: A combined effect of condensational heating and synoptic eddy activities

**Shengjie Chen**
  Nanjing University

**Xiu-Qun Yang** ( ✉ xqyang@nju.edu.cn )
  Nanjing University

**Jiabei Fang**
  Nanjing University

**Linyuan Sun**
  Nanjing University

**Lingfeng Tao**
  Nanjing University

**Xiaozhuo Sang**
  Nanjing University

**Manman Yin**
  Nanjing University

**Additional Declarations:** No competing interests reported.

# Abstract

The East Asian summer monsoon (EASM) is a unique regional monsoon in the subtropics involving not only tropical but midlatitude processes. Most of the previous studies identified the role of condensational heating which is largely relevant to the tropical moisture transport in determining the dynamical structure of EASM. However, how midlatitude synoptic eddy activities can affect the EASM structure has not been well recognized. With dynamical diagnoses, this study revisits the EASM structure by emphasizing the roles of feedbacks of condensational heating versus synoptic eddy activities. As EASM is characterized by a grand low-level low with strong humid southerly flows extending from the tropics to the northeastern Asia, its vertical structure is found to have a distinct meridional difference bounded at around 35.5°N. In the southern domain, EASM features a meridional overturning cell and a baroclinic structure with an upper-level high versus a lower-level low in geopotential height, which are primarily controlled by substantial condensational heating due to abundant monsoon precipitation. However, in the northern domain, EASM exhibits an equivalent barotropic structure with an upper-level low versus a lower-level low. Such a unique structure results from a combined effect of feedbacks of condensational heating and synoptic eddy activities, in which the upper-level low is dominated by the synoptic eddy dynamical feedback while the lower-level low is induced by the both feedbacks. The role of the midlatitude transient eddy activities in shaping the EASM structure proposed in this study provides a new perspective for understanding the formation and variation of EASM.

# 1. Introduction

The East Asian summer monsoon (EASM) is a distinctive and prominent regional component of the grand Asian summer monsoon system which features a prominent seasonal reversal of prevailing winds and an abrupt change from dry to wet climate (Ramage 1971; Tao and Chen 1987; Wester and Yang 1992; Lau 1992; Ding 1994; Wester et al. 1998; Lau et al. 2000; Li and Zeng 2003; Wang et al. 2011, 2012; An et al. 2015). Substantial variation of EASM can cause weather and climate disasters in the densely populated East Asia (Wang et al. 2005; He et al. 2007; Ding et al. 2008, 2009; Chang et al. 2012; Li et al. 2016; Zhou et al. 2018).

Like the South Asian summer monsoon, another subcomponent of the Asian summer monsoon system, the EASM flows mainly come from tropical regions. However, EASM cannot be just considered as the eastward and northward extension of the South Asian summer monsoon (Zhu 1934; Yeh et al. 1957; Zhu et al. 1986; Tao and Chen 1987; Lau et al. 2000; Ding and Chan 2005; Huang et al. 2017). EASM can bring abundant moisture and rainfall by intense low−level southerlies from the tropics towards midlatitudes (Tao and Chen 1987; Ding et al. 1994; He et al. 2007; Lau et al. 2000; Wang and Lin 2002; Wang et al. 2004). Meanwhile, EASM is also closely related to the midlatitude circulation systems. The EASM rainybelt is intimately associated with the frontal zone where the northward warm−moist flow meets with the cold air from the mid−high latitudes. Thereby, in addition to the tropical and subtropical circulation systems such as the monsoonal trough and the subtropical high, the mid−high latitude troughs and ridges that can affect the thermal and dynamical conditions of EASM should also be considered in the complete EASM system (Ding and Chan 2005; He et al. 2007; Ding et al. 2018). Given those natures, Wang and Lin (2002) defined the

EASM domain within 20º–50ºN and 110º–140ºE, a region mostly in the subtropics, distinguishing it from the South China Sea summer monsoon. And even, Molnar et al. (2010) insisted that EASM should be defined as a frontal system rather than a "monsoon" in terms of its distinctly extratropical natures. No matter what way of the identification, it comes to an agreement that EASM is extremely complicated for its hybrid natures.

To understand the complex natures of EASM, great efforts have been made to investigate the formation mechanisms responsible for EASM. Most of the previous studies identified the roles of various thermal processes in the EASM formation, in which the seasonal variation of solar radiation (Halley 1686; Tao and Chen 1987; Ding 1994; Lau et al. 2000; Li and Zeng 2003; Zhao and Wang 2014) and the thermal contrast between land and ocean (Luo and Yanai 1983; Li and Yanai 1996; Sun et al. 2001; Liang et al. 2006; Qi et al. 2008) are widely believed to be the two fundamental thermal factors. The elevated sensible heating by the Tibetan Plateau is proposed to be another factor for the monsoon formation (Ye 1981; Ye and Wu 1998; Yeh 1982; Wu and Liu 1998; Wu and Zhang 1998; Ueda and Yasunari 1998; Ye and Wu 1998; Liu et al. 2001, 2012; Yanai and Wu 2006; Kripalan et al. 2010; Molnar et al. 2010; Qiu 2013; Ma et al. 2014; Wu et al. 2007, 2012a, 2012b, 2015a, 2018). Besides, the deep condensational heating generated from the latent heat release of monsoonal rainfall dominates the diabatic heating over East Asia and feedbacks onto the EASM itself (Jin et al. 2013). The feedback of condensational heating is not only in favor of the South China Sea summer monsoon onset (Liu et al. 2002; Wen et al. 2004), but also contributes to the amplification and maintenance of the EASM circulation (Li and Luo 1988; He et al. 1989; Wu and Liu 1998; Wu et al. 1999; Liu et al. 2002, 2004; Wen et al. 2004). Based on numerical experiments, Jin et al. (2013) confirmed that the condensational heating feedback caused by monsoon rainfall acts to largely enhance low–level flows of the EASM and essentially determine its baroclinic vertical structure and meridional cell, once the solar radiation and the inhomogeneity of the Earth's surface induce low–level monsoon flows in East Asia by enhancing land–sea thermal contrast.

However, as the EASM flows march northward into the midlatitudes, EASM exhibits some midlatitude characteristics (Tao and Chen 1987; Zhang and Tao 1998; Wu 2002; Ding and Chan 2005). The midlatitude circulation favors the vigorous genesis of synoptic transient eddies which can feedback onto the mean flow through redistributing the momentum and heat (Holopainen et al. 1982; Lau and Oort 1982; Lau and Holopainen 1984; Luo 2005a, 2005b; Luo et al. 2007; Ting et al. 2001; Zhang et al. 2009). Various previous studies pointed out the importance of transient eddy feedback to the seasonal–mean atmospheric circulation anomalies (Nakamura et al. 2002; Chen et al. 2013; Leung and Zhou 2015; Fang and Yang 2016). Although transient eddy activities are relatively weak in summer, there is increasing evidence showing significant impacts of transient eddy activities on EASM and the associated climate anomalies. For example, active transient eddies at mid–high latitudes tend to enhance the rainfall in the Yangtze–Huaihe River Basin by inducing more southward invasion of cold air (Tan 2008; Dong et al. 2006). Synoptic–scale geopotential height anomalies in the upper troposphere and temperature anomalies in the mid–lower troposphere are the early signals for the summer low–temperature events in northeastern China (Qian et al. 2014). Anomalous transient eddy activities in summer can induce the anomalous southerlies over eastern China (Park et al. 2015), the interannual meridional displacement of the East Asian subtropical jet (Xiang and Yang 2012), and the decadal changes of EASM around the early 1990s (Chen et al. 2016).

Since the warm and humid southerlies of EASM can meet the cold and dry northerlies, that is the front genesis, in the midlatitudes, the atmospheric baroclinicity enhances, favoring synoptic transient eddy activities. Whether and how the transient eddy can feedback onto EASM have not been well explored before. In this study, we try to revisit the EASM structure in which the roles of feedbacks of condensational heating versus synoptic eddy activities are particularly identified through dynamical diagnoses in terms of the seasonal mean quasi−geostrophic potential vorticity equation (Holton 1979; Lau and Holopainen 1984; Fang and Yang 2016). The rest of paper is organized as follows. Section 2 describes the data and methods used. Section 3 presents a complete picture of the EASM structure. Section 4 and Section 5 explore the roles of feedbacks of condensational heating and transient eddy activities in the EASM structure, respectively. The final section is devoted to conclusions and discussion.

## 2. Data And Methods

### a. data

The 6−hourly circulation variables including geopotential height, temperature, winds, and vertical velocity are obtained from the Japanese 55−yr Reanalysis (JRA−55) dataset conducted by the Japan Meteorological Agency (Kobayashi et al., 2015). The reanalysis dataset comprises 23 vertical levels between 1000 hPa to 200 hPa with a fine horizontal resolution of 1.25°×1.25°. Additionally, the diabatic heating components due to longwave radiation, solar radiation, large−scale condensation, convective condensation, and vertical diffusion, respectively, are derived from the JRA−55 dataset. The global daily precipitation dataset with a horizontal resolution of 0.5°× 0.5° is part of products suite from the National Oceanic and Atmospheric Administration (NOAA) Climate Prediction Center Unified Precipitation Project (Xie et al. 2007). The daily large scale and convective precipitation rate data is taken from the Climate Forecast System Reanalysis (CFSR) reanalysis dataset with a spatial resolution of 0.5°×0.5° provided by the National Centers for Environmental Prediction (NCEP) (Saha et al. 2010). All the variables and their derivatives are averaged for summer (June, July and August) with a time span for 1980−2019. In addition, to isolate the regional characteristics of EASM, the regional departure circulations over the East Asian domain are extracted through removing globally zonal means.

### b. methods

In the extratropics, the seasonal mean atmospheric state is approximately governed by the quasi−geostrophic potential vorticity (QGPV) equation (Fang and Yang, 2016) which is written as,

$$\left(\frac{\partial}{\partial t} + \bar{\vec{V}}_h \cdot \nabla\right)\left[\frac{1}{f}\nabla^2\bar{\Phi} + f + \frac{\partial}{\partial p}\left(\frac{f}{\bar{\sigma}_1}\frac{\partial\bar{\Phi}}{\partial p}\right)\right] = -fR\frac{\partial}{\partial p}\left(\frac{1}{\bar{\sigma}_1}\frac{\bar{Q}_d}{p}\right) - fR\frac{\partial}{\partial p}\left(\frac{1}{\bar{\sigma}_1}\frac{\bar{Q}_{eddy}}{p}\right) + \bar{F}_{eddy}$$

1

,

where the overbar denotes the seasonal mean, $\Phi$ is the geopotential, $\bar{V}_h$ is the horizontal wind, $T$ is the temperature, $f$ is the ambient vorticity, $R$ is the gas constant for dry air, and $\sigma_1$ is the static stability parameter which varies only with altitude ($\sigma_1 = -\alpha \cdot \partial \ln \theta / \partial p$, $\theta$ is the geopotenial temperature, $\alpha$ is the reciprocal of atmospheric density). $\bar{Q}_d$ is the seasonal–mean diabatic heating induced by longwave radiation, shortwave radiation, large–scale condensation, convective condensation, and vertical diffusion. $\bar{Q}_{eddy}$ and $\bar{F}_{eddy}$ are the seasonal mean heating and vorticity forcing, respectively, induced by high–frequency transient eddy activities, which are expressed as,

$$\bar{Q}_{eddy} = -\nabla \cdot \overline{\vec{V}_h' T'} - \frac{\partial \overline{\omega' T'}}{\partial p} + \frac{R}{c_p p} \overline{\omega' T'}, \tag{2}$$

$$\bar{F}_{eddy} = -\nabla \cdot \overline{\vec{V}_h' \varsigma'}, \tag{3}$$

where the prime denotes the 2−10d synoptic disturbances obtained with a Lanczos filter (Duchon 1979). $\omega$, and $\varsigma$ are the vertical velocity and the relative vorticity, respectively. Obviously, $\bar{Q}_{eddy}$ and $\bar{F}_{eddy}$ are determined by the convergences of synoptic transient eddy heat and vorticity fluxes, respectively.

To identify the effects of the diabatic heating and the transient eddy forcing on mean flow, Eq. (1) can be re−written as,

$$[\frac{1}{f}\nabla^2 + f\frac{\partial}{\partial p}(\frac{1}{\bar{\sigma}_1}\frac{\partial}{\partial p})]\frac{\partial \bar{\Phi}}{\partial t} =$$

$$\underbrace{-\vec{V}_h \cdot \nabla[\frac{1}{f}\nabla^2 \bar{\Phi}]}_{A_1} \underbrace{-\beta \bar{v} -\vec{V}_h \cdot \nabla[\frac{\partial}{\partial p}(\frac{f}{\bar{\sigma}_1}\frac{\partial \bar{\Phi}}{\partial p})]}_{A_2 \qquad A_3} \underbrace{-fR\frac{\partial}{\partial p}(\frac{1}{\bar{\sigma}_1}\frac{\bar{Q}_d}{p})}_{F_1} \underbrace{-fR\frac{\partial}{\partial p}(\frac{1}{\bar{\sigma}_1}\frac{\bar{Q}_{eddy}}{p})}_{F_2} \underbrace{+\bar{F}_{eddy}}_{F_3}$$

4

,

the left−hand side of Eq. (4) represents the tendency of QGPV with a three−dimensional linear operator acting on the tendency of geopotential. On the right−hand side, there are three forcing terms producing atmospheric potential vorticity, which are the diabatic heating forcing term ($F_1$), the transient eddy heating forcing term ($F_2$), and the transient eddy vorticity forcing term ($F_3$). There are also three vorticity advection terms associated with atmospheric internal processes, which are the relative vorticity advection ($A_1$), the ambient vorticity advection ($A_2$), and the stretching vorticity advection ($A_3$). For the climatological state of the atmospheric circulation, the tendency of QGPV is nearly zero and thus the vorticity advection terms can be considered as the adjustment to or the balance with the vorticity production terms. The seasonal−mean geopotential tendencies produced by those terms on the right−hand side of Eq. (4) can be numerically solved with the three−dimensional linear operator on the left−hand side of Eq. (4) by the successive

overrelaxation (SOR) method with the boundary conditions referred to Lau and Holopainen (1984). Therefore, the roles of diabatic heating and transient eddy forcing in the EASM structure can be examined through analyzing these tendencies.

The high-frequency transient eddy activity is closely related to the low-level atmospheric baroclinicity (Hoskins and James, 2014; Simmons and Hoskins, 1978), which is represented approximately by the maximum Eady growth rate $\sigma_{BI}$ (Lindzen and Farrell 1980; Hoskins and Valdes 1990; Vallis 2006). It is defined as $\sigma_{BI} = 0.31 f \left| \partial \vec{V}_h / \partial z \right| / N$, where $N = (g \left| d\theta/dz \right| / \theta^{1/2})$ is the $\mathrm{Brunt - V\ddot{a}is\ddot{a}l\ddot{a}}$ frequency. The intensity of the synoptic-scale eddy activity can be characterized by the eddy available potential energy (EAPE) and the eddy kinetic energy (EKE), which are defined as $EAPE = (C_p \tau)(\overline{T'^2})/2$ and $EKE = \overline{(u'^2 + v'^2)}/2$, respectively, where $\tau = -R/(pC_p)(p_0/p)^{R/C_p}(\partial\theta/\partial p)^{-1}$ is an inverse measure of the background stratification (Lorenz 1955), $C_p$ is the specific heat capacity of dry air at the constant pressure and $p_0 = 1000 hPa$ is the mean sea level pressure.

# 3. Three-dimensional Structure Of Easm

The climatology of the summertime precipitation rate and monsoon wind are shown in Fig. 1. As shown in Fig. 1a, the monsoonal circulation over East Asia exhibits a distinct seasonal reversal, characterized by the prevailing low-level winds changing from the wintertime northerlies to the summertime southerlies (vectors in Fig. 1a). In summer, the westerlies and southwesterlies from the tropics converge with the southeasterlies from the Northwest Pacific and then turn northward together over the South China Sea. The development of monsoonal southerlies is followed by the northward shift of rainbelt, producing abundant precipitation over China, Korea, south-central Japan, and even Northeastern Asia (Fig. 1a). Many studies argued that the subtropical high pressures over the Northwest Pacific and North Pacific play a key role in the formation and maintenance of monsoonal southerlies. After removing the globally zonal means, a grand cyclonic circulation deviation naturally occurs, replacing the wintertime anticyclone over the East Asian continent at the low levels. The regional monsoonal low represents the localized feature of EASM without being influenced by seasonal variation of solar radiation, and thus, it is natural to believe that the strong monsoonal southerlies are not only related to the North Pacific subtropical high but also closely connected with the grand monsoonal low over the East Asian continent (Fig. 1b).

Upon the grand low-level monsoonal low, there is a distinct meridional difference of the vertical structure bounded at around 35.5ºN. The monsoonal low south of 35.5ºN is overlain by a regional high deviation with anticyclonic circulation centered over the Tibet Plateau at the upper level, featured by a baroclinic structure. This high deviation is just the zonal asymmetry component of the South Asia high, an indispensable member of the EASM system that has been paid much attention to. While north of 35.5ºN, the regional low deviation with cyclonic circulation dominates in the whole monsoonal low, presenting an equivalent barotropic structure (Fig. 2b). This upper-level low deviation superimposed on the basic westerlies has been got less emphasis before. Interestingly, the location of the upper-level seasonal mean low deviation is just where the synoptic Northeast cold vortex often occurs.

The meridionally different vertical structures are further confirmed by the longitude–height profile of geopotential height along 105–135°E (Fig. 3a). In the southern domain of EASM, the geopotential height structure shows clear baroclinic features with negative deviation at the lower level and positive deviation at the upper level. However, in the northern domain, a low–pressure deviation with an equivalent–barotropic structure is distinguished from the southern baroclinic structure and the northern barotropic high–pressure. According to the geostrophic relationship, the boundaries separating the three different vertical structures are the barotropic westerly and easterly deviations with the centers at 35.5°N and 50.5°N, respectively (Fig. 3a). The difference in the thermal field is also clear that regional warm air almost occupies the whole troposphere with the mid–level warm center at 300 hPa in the southern domain, while the warmer air is nearby the surface in the northern domain (Fig. 3b), which is in accordance with the static equilibrium relationship between the geopotential height and temperature.

Regarding the wind field, in the southern EASM domain, the southerly deviation at the mid–low level is overlaid by the northerly deviation at the upper troposphere, dynamically consistent with the baroclinic structure of geopotential deviation here (Fig. 4). And the significant ascending flows control the whole troposphere, forming a grand thermal indirect cell over the East Asian sector with major ascending flows centered roughly at 15°N, 22.5°N, and 30°N (Figs. 4a, 5a). This three–dimensional circulation structure accords well with the thermal adaption theory that highlights the positive vertical shear of meridional flows is proportional to the ascending movement at steady motion (Liu et al. 2001; Wu et al. 1999, 2007). However, the strong updraft and the monsoonal overturning cell are weakened at around 35.5°N, manifested by a very slight indirect cell at the mid–lower troposphere over the section of 35.5–50°N (Figs. 4, 5), which is due to the cancellation between the northward ascending motion and the southward descending motion to the east and west of 120°E, respectively. Obviously, the circulation cell structure over Northern East Asia distinguishes it from that in the southern EASM and cannot be described by the thermal adaption theory.

The observational fact that a transition zone of the large–scale condensational and convective precipitation just appears at about 34°N is another evidence for the longitudinal difference in the dynamics of the circulations over the southern and northern EASM regions. Evidently, the convective precipitation dominates the region equatorward at around 34°N, while the rainfall to the north of 34°N is frequently triggered by the large–scale lifting motion (Fig. 6).

Overall, a revisit on the three–dimensional structure of EASM suggests that the complete EASM regime is complicated and bears two different vertical structures in the longitudinal direction, although being under the control of a grand monsoonal low near the surface. One is a baroclinic structure with an upper–level high versus a lower–level low in the southern domain. The other is an equivalent barotropic structure with almost no vertical tilt low in the geopotential height over the troposphere in the northern domain. The baroclinic structure is widely considered as the traditional monsoonal feature of opposite polarity and has proved to be attributed to the role of condensational heating. While the barotropic vertical structure over northern East Asia implies the effect of midlatitude dynamics, in which the detailed dynamical processes have not been well recognized. The mechanisms responsible for the vertical structure in the northern domain and the difference from that in the southern domain should be further explored.

Given that, we attempt to understand the formation of the unique vertical structure of EASM, focusing on the role of the diabatic heating and synoptic eddy activities by dynamical diagnoses on the quasi-geostrophic potential vorticity (QGPV) equation (Eq. 1).

## 4. Role Of Feedback Of Diabatic Heating In Easm Structure

As illustrated in Fig. 7a, the diabatic heating warms up the almost entire tropospheric air column (except some layers below 850 hPa equatorward of 40°N) with centers at about 400 hPa over the tropics, the subtropics, and the midlatitudes. As strong EASM brings out abundant water vapor and consequently generates substantial latent heat release, the condensational heating considerably dominates the diabatic heating in summer along the East Asia sector (Fig. 7). The condensational heating is deep and totally determines the diabatic heating in the southern EASM domain (Fig. 7c), while in the northern domain, the diabatic heating is much weaker and presents two heating centers, in which one is in the boundary layer attributed to the strong land surface sensible heat flux (Fig. 7d) and the other is at the mid-troposphere due to the latent heat release (Fig. 7c).

In terms of Eq. (1), the diabatic heating centered at 400 hPa would produce a positive (negative) potential vorticity source, consequently exciting a negative (positive) geopotential tendency below (above) 400 hPa, which is supported by the numerically-solved results of geopotential tendency (Figs. 8, 9). The baroclinic atmospheric response with a negative (positive) geopotential tendency below (above) 400 hPa is induced by the diabatic heating forcing at the middle layers, coinciding well with the observed baroclinic vertical structure of geopotential height in the southern EASM domain. Thus, it can be concluded that the diabatic heating forcing that mainly comes from the latent heat release amplifies the steady baroclinic vertical structure in the southern EASM once EASM is initially driven. This thermodynamic relationship is classical and has been widely reported in previous studies (Jin et al. 2013; Liu et al. 2001; Wu et al. 1999, 2007).

In the northern domain, since there are two heating centers, both could produce a positive (negative) potential vorticity below (above) the centers. However, the eventual inversion result presents a baroclinic atmospheric response with a negative geopotential tendency below versus a positive geopotential tendency upon 500 hPa (Figs. 8, 9). The induced low response by the local diabatic heating is relatively weak and confined at the lower troposphere. The induced high response covers the upper troposphere (Figs. 8, 9), which contradicts the observed equivalent barotropic structure with an upper-level low upon a lower-level low (recall Fig. 3). In other words, if only considering the role of diabatic heating, the vertical structure in the northern domain should be a steady baroclinic structure with an upper-level high versus a lower-level low in geopotential height once EASM onsets with the latent release heating the mid-troposphere as that over the southern domain. Obviously, it is inconsistent with reality (Fig. 8b).

Through dynamical diagnoses, it is further verified that diabatic heating, especially condensational heating makes a crucial role in dynamically determining the baroclinic structure of EASM, consistent with many previous studies. However, the feedback of the diabatic heating cannot explain the equivalent barotropic structure north of 35.5°N in the EASM regions. Considering that the EASM dynamics include synoptic transient eddy activities in the midlatitudes, such as the transient eddy feedback, which also serves as

important forcing terms in Eq. (1), attracts us to further explore how it contributes to the observed three–dimensional EASM structure.

# 5. Role Of Feedback Of Synoptic Eddy Activities In The Easm Structure

As the most common weather phenomenon in the mid–latitudes, frequent synoptic–scale transient eddies can act as an internal atmospheric factor to maintain or change the time–mean flow through generating potential vorticity sources as the diabatic heating does (Holopainen et al. 1982; Lau and Oort 1982; Lau and Holopainen 1984). According to the right–hand terms of Eq. (1), there are two forcing terms associated with transient eddy activities: the transient eddy heating forcing term ($F_2$), and the transient eddy vorticity forcing term ($F_3$). The former is proportional to the vertical gradient of the transient eddy heating, and the latter is determined by the divergence of transient eddy vorticity flux. Clearly, the transient eddies influence the atmospheric state by redistributing heat and vorticity.

Relationships between the atmospheric transient eddy activities and the mean flow were previously identified with zonal averages over the whole Northern Hemisphere from the climatological view (Holopainen et al. 1982; Lau and Holopainen 1984). Fang and Yang (2016) has found out that the atmospheric transient eddy is an indispensable ingredient that provides a positive feedback mechanism for the unstable ocean–atmosphere interaction in the midlatitude North Pacific. Here, we try to reveal the effect of transient eddy forcing on the barotropic structure of monsoonal circulation in the northern EASM domain.

# 5.1 Features of synoptic eddy activities

Climatologically, the summertime westerly has a maximum located around 40 °N at the upper troposphere, showing the typical feature of the subtropical westerly jet stream over Asia (Fig. 10a). Due to the strong vertical wind shear and meridional temperature gradient around the jet, the extratropical baroclinic nature over the EASM domains is evident. The maximum Eady growth rate $\sigma_{BI}$ (Lindzen and Farrell, 1980), representing the growth of the atmospheric baroclinic instability, has a maximum over those zones around and north of 40°N over northwestern East Asia (Fig. 10a). It implies the stronger genesis of the synoptic eddies and the tendency of producing more eddy available potential energy (EAPE). Consistent with the stronger low–level atmospheric baroclinicity, the EAPE maximizes around the 40°N over northwestern East Asia at the mid–lower troposphere (Fig. 10b), further confirming the stronger genesis of transient eddy activities. As the development and movement of the generated synoptic eddies, the highest cyclone frequency and the maximum eddy kinetic energy (EKE) are located at around 30°–50°N over Northeast Asia in the upper troposphere. It is suggested that upper–level transient activities develop and further enhance in downstream of the eddy genesis region. Correspondingly, accompanied by the enhancement of eddy activities, the eddies exert forcing on the mean flow via redistributing heat and momentum through eddy heat flux ($\overline{v'T'}$) (Fig. 10e) and eddy momentum flux ($\overline{u'v'}$) (Fig. 10f). Figure 10e shows that the poleward transient eddy heat flux mainly occurs across the jet and maximizes around 40°N, producing a cooling (heating) effect south (north) of the jet axis at the upper troposphere. Meanwhile, the transient eddy momentum flux presents the poleward and equatorward transport to the south and north of the jet stream

respectively, and the strongest poleward momentum flux occurs at around 30º−40ºN, causing the convergence of eddy momentum flux nearby. According to the zonal−mean momentum balance (Hoskins et al. 1983), such a pattern of transient eddy momentum flux favors accelerating the time−mean westerly flow around 40−50ºN.

So generally, in the northern EASM domain, the summertime transient eddies are generated over northwestern East Asia and then strengthen downstream over Northeast Asia (around 30º−50ºN), and thus, the synoptic eddies activities could effectively affect the mean circulation over Northeast Asia via redistributing the atmospheric heat and momentum.

## 5.2 Feedback of synoptic eddy activities

In agreement with the horizontal distribution of transient eddy heat flux at 300 hPa (Fig. 10e), the level−latitude profile of the seasonal mean transient eddy heating forcing $\bar{Q}_{eddy}$ shows the cooling (heating) effect south (north) of around 40ºN throughout the mid−upper troposphere above 800 hPa (Fig. 11a). In terms of the transient eddy heating forcing term ($F_2$) in right of Eq. (1), positive (negative) vertical gradient of $\bar{Q}_{eddy}$ is the source of the positive (negative) PV. For the subtropical region over the 30−40ºN, the middle−tropospheric cooling effect (centered at around 400 hPa) dominates the vertical structure (Fig. 11a), so based on Eq. (1), it will cause a positive (negative) PV tendency at the low (upper) levels. After solving the seasonal−mean geopotential tendency induced by the transient eddy heating forcing, a vertically baroclinic structure of the atmospheric response is obtained and manifested with the positive geopotential tendency at the low level versus the negative at the upper level (Fig. 11c). Such a vertical structure is opposite to that induced by the seasonal−mean diabatic heating, especially over the latitudes of 30º−40ºN (Figs. 8b, 11c). The horizontal distribution of the geopotential tendency induced by transient eddy heating forcing as seen in Fig. 12 further suggests that the cooling effect by the transient eddy heat transport could yield a baroclinic vertical structure with a high−level decreased versus a low−level increased geopotential over the most East Asia Continent. The role of the transient eddy heat forcing partly offsets that of the diabatic heat forcing on the seasonal−mean circulation structure of EASM.

The transient eddy activities also influence the atmospheric state by redistributing vorticity. Over East Asia, the local transient eddy vorticity flux convergence produces a positive PV source at around 20º−35ºN and 40º−55ºN throughout the troposphere with large values above 400 hPa (Fig. 13a). In terms of Eq. (1), the transient eddy vorticity forcing is also one of the PV sources for the seasonal−mean atmosphere, and accordingly, numerical solution shows that the transient eddy vorticity forcing induces the negative geopotential tendency with an equivalent−barotropic (maximized at the upper level) over the two zones (20º−35ºN and 40º−55ºN) (Fig. 13b). Although the negative geopotential tendency induced by the transient eddy vorticity forcing can also be partly offset by the positive geopotential tendency induced by diabatic heating forcing at upper levels, in general, the equivalent−barotropic negative geopotential tendency accords well with the observed equivalent−barotropic low−pressure deviation in the northern EASM domain (Figs. 13b, 14).

Both the diabatic heating and transient eddy vorticity forcing contribute to the equivalent−barotropic low pressure at low levels in the northern EASM domain. At upper levels, it is mainly the transient eddy vorticity forcing that plays a major role in the formation of observed low pressure. However, if we carefully check Figs. 13 and 14, it is noticed that the positive PV source and negative geopotential tendency induced by the transient eddy vorticity forcing are centered at around 47.5°N, obviously shifting northward by about 5 latitudes and somewhat westward compared with the observed low pressure. When further considering the conservative process associated with the adjustment to or the balance with the vorticity production terms, the location shift of the initial response to the transient eddy vorticity forcing from the ultimate balanced circulation structure can be interpreted. As seen in Fig. 15, three types of advection processes, as introduced in the method in section 2, could affect the final position of the initial atmospheric response to the transient eddy vorticity forcing. One is the relative vorticity produced by the transient eddy vorticity forcing advected by the globally zonal mean flow ($-\dfrac{U}{f}\dfrac{\partial \nabla^2 \bar{\Phi}_{t,\overline{F}\,eddy}}{\partial x}$), where $U$ is the globally zonal mean zonal winds, $\bar{\bar{\Phi}}_{t,\overline{F}\,eddy}$ is the geopotential tendency induced by the transient eddy vorticity forcing. It is seen in Fig. 15a that this advection effect makes the negative geopotential tendency by the transient eddy vorticity forcing shift eastward and southward. Another is the advection effect of the basic zonal flow on the stretching vorticity, and the corresponding calculation formula is as $-U\dfrac{\partial}{\partial x}\left[\dfrac{\partial}{\partial p}\left(\dfrac{f}{\sigma_1}\dfrac{\partial \bar{\Phi}_{t,\overline{F}\,eddy}}{\partial p}\right)\right]$. Similar to the former advection effect, the stretching vorticity−related advection effect also contributes to the eastward and southward shift of the initial geopotential tendency induced by the transient eddy vorticity forcing. More specifically, the eastward shifting is attributed to the decreasing of the perturbed relative vorticity and stretching vorticity by the transient eddy vorticity forcing with longitude. The southward shifting is due to the inhomogeneity of the globally zonal mean zonal flow at the meridional direction with the center at around 43°N, what is just located southward of the center of the negative tendency induced by the transient eddy vorticity forcing (Fig. 15c). The last advection process is the ambient vorticity advected by the meridional flows induced by the transient eddy vorticity forcing, that is calculated by $-\dfrac{\beta}{f}\dfrac{\partial \bar{\Phi}_{t,\overline{F}\,eddy}}{\partial x}$. Under the geostrophic relationship, the negative geopotential tendency by the transient eddy vorticity forcing corresponds to a southerly tendency in the east and a northerly tendency in the west, thus yielding the southward and northward transport of the ambient vorticity, respectively. This advection effect leads to the westward shifting of the initial perturbed low pressure (Fig. 15b). In general, the position shifting between the low pressure in the equilibrium state and the initial negative geopotential tendency induced by the transient eddy vorticity forcing is mainly attributed to the advection of the perturbed relative vorticity and stretching vorticity by the globally zonal mean flow. Therefore, different from the dynamics for tropical circulation in the southern EASM domain that the vorticity changes induced by the diabatic heating are mainly balanced by the meridional advection of the ambient vorticity, the midlatitude circulation in the northern EASM domain is mainly subjected to the QGPV dynamics that the induced vorticity tendency by the transient eddy vorticity forcing is balanced by the advection of the relative vorticity and stretching vorticity by the globally zonal mean flow.

# 6. Conclusions And Discussion

As a prominent and independent component of the grand Asian summer monsoon system, EASM features a huge monsoon low over the East Asian continent and a seasonally northward march of intense southerly flows. The huge monsoonal low has been attributed to the seasonal variation of solar radiation and the associated thermal contrast between the Asia Land and the Pacific Ocean. The influence of the dynamical and thermal forcing by the Tibetan Plateau is another mechanism for the EASM formation. However, these explanations are still incomplete in understanding the physical processes of the EASM formation. Recent evidence has recognized that diabatic heating, especially the atmospheric condensational heating associated with moisture processes, could contribute to the formation and maintenance of EASM. In our study, there is a reasonable hypothesis that the feedback of synoptic eddy activities also plays an indispensable role in the complete EASM regime.

A revisit on the three−dimension circulation structure of EASM suggests that upon the grand low−level monsoonal low with strong humid southerly flows extending from the tropics to Northeast Asia, there exists a distinct meridional difference in the vertical structure of EASM with a boundary of around $35.5^{\circ}$N. In the southern domain, EASM features a meridional overturning cell and a baroclinic structure with an upper−level high versus a lower−level low in geopotential height. While in the northern domain, the EASM exhibits an equivalent barotropic structure with an upper−level low versus a lower−level low, and the ascending accompanied with the northward motion and the descending with southward motion dominate to the east and west of $120^{\circ}$E over northeastern Asia, respectively. Such differences in the three−dimensional structures imply some different dynamics over the two domains.

What are the physical processes responsible for the formation of circulation systems with different vertical structures of EASM? Here, we answer it by focusing on the feedbacks of diabatic heating and synoptic eddy activities by diagnosing the QGPV equation, a powerful tool for identifying the seasonal−mean atmospheric response to the forcing. Regardless of friction, the diabatic heating as well as the transient eddy heat and vorticity transport are all important sources of forcing terms on the time−mean flow. The diabatic heating and the transient eddy heating forcing are both the thermal effect on the mean flow and could induce baroclinic geopotential tendencies. Differently, the geopotential tendencies induced by the transient eddy vorticity forcing present the equivalent−barotropic vertical structure.

Consistent with previous results, the baroclinic monsoonal circulation in the southern EASM domain is dynamically determined by diabatic heating, especially condensational heating. Specifically, the mid−tropospheric diabatic heating would induce the baroclinic circulation response characterized by the positive PV and negative geopotential tendency at the low level versus the negative PV and positive geopotential tendency at the upper level. By the advection effect of meridional wind on the ambient vorticity, the circulation response to the diabatic heating tends to shift westward, and then, in the final state of equilibrium, the southerly wind prevails at the lower level and the northerly wind prevails at the upper level. Thereby, a local meridional cell dominates over the southern EASM region and becomes a part of the tropical monsoonal circulation south of $20^{\circ}$N.

However, in the northern domain of EASM, if only considering the effect of diabatic heating, a regional high should prevail above the monsoonal low and the northern low is only confined to the lower troposphere,

while this is clearly inconsistent with the observational fact, so we try to emphasize the role of the transient eddy forcing in the formation of the observed equivalent−barotropic low pressure here. In summer, the northern EASM region experiences strong heat and vorticity transport by synoptic transient eddies, which in turn feedback on the time−mean flow. The transient eddy heat flux diverges over the south of 40°N, yields the cooling effect on the middle troposphere, and consequently induces a distinct baroclinic structure with an upper−level low and a lower−level high tendency in the northern EASM. The structure of atmospheric response induced by the transient eddy heating forcing is exactly opposite that induced by the diabatic heating forcing, suggesting that the mid−tropospheric cooling effect by the transient eddy heat forcing might partly offset the diabatic heating forcing. However, the transient eddy vorticity forcing could produce a negative geopotential tendency centered at the upper layers with a barotropic vertical structure. Although the center of the initial atmospheric response induced by the transient eddy vorticity forcing lies northwest to the observed barotropic low over northeastern Asia, due to the adjustment of the relative vorticity and stretching vorticity advected by the globally zonal mean zonal flow, the initial atmospheric geopotential tendency induced by the transient eddy vorticity forcing could deviate from the initially−formed area and shift southeastward, and eventually, coincide with the observed regional barotropic low. Combined with the effect of the diabatic heating on the low−level flow, there presents a distinct vertical structure of regional low centered roughly at 42.5°N with deep southerlies and upward motion in the east and deep northerlies and downward motion in the west in the northern domain.

In summary, we conclude that in the complete EASM regime, the feedbacks of diabatic heating and transient eddy forcing are both important and nonnegligible mechanisms responsible for the formation of EASM. The vertical circulation structure over the southern EASM region is mainly determined by the impact of the diabatic heating that mainly comes from the local latent heating. However, the steady vertical structure of the northern EASM is attributed to the combined effect of the feedbacks of diabatic heating and synoptic eddy activities. Especially, in the northern EASM domain, the formation of the equivalent−barotropic circulation system at the mid−upper troposphere is induced by the synoptic transient eddy vorticity forcing.

Indeed, the role of transient eddy forcing on the formation of the summertime low-level low pressure in the northern EASM has also been noticed by Lin et al. (2021). Although their result shows that the effect of transient eddy forcing is negligible for the formation of Northern East Asia Low based on a linear baroclinic model with simplified physical processes and omitted non−linear interactions, Lin et al. (2021) has already realized some limits on their study and recognized the underestimation of the effect of transient eddy forcing. This underestimation is because the coarse−resolution reanalysis cannot resolve synoptic eddies sufficiently (Sang et al. 2021). Therefore, even though the feedback of transient eddy activities is somewhat weaker than that of diabatic heating in quantity, we still believe that the transient eddy, especially the transient eddy dynamical feedback works on the formation of the EASM structure in the northern domain.

The role of the midlatitude transient eddy activities in shaping the EASM structure gives us new insights into understanding the formation and variation of EASM from the perspective of wave−mean flow interactions. This study only focused on the transient eddy feedback on the summertime mean state of the East Asian monsoon system. How the transient eddy feedback affects the seasonal evolution, interannual and other

timescale variabilities of EASM are still open questions, which need further deep exploration to improve the research on variation and prediction of EASM.

# Declarations

### Ethics approval and consent to participate

The authors follow the rules of good scientific practice.

### Consent for publication

Written informed consent for publication was obtained from all participants.

### Availability of data and material

The Japanese 55–year Reanalysis (JRA–55) is available at https://climatedataguide.ucar.edu/climate–data/jra–55. The Climate Forecast System Reanalysis (CFSR) is achieved from https://climatedataguide.ucar.edu/climate–data/climate–forecast–system–reanalysis–cfsr. The global daily precipitation data set from   NOAA Climate Prediction Center (CPC) is available at https://downloads.psl.noaa.gov/Datasets/cpc_global_precip/.

### Competing interests

The authors have no relevant financial or non–financial interests to disclose.

### Authors' contributions

All authors contributed to the study conception and design. The main idea of the study was put forward by XQY. Material preparation, data collection and analysis were performed by SC and XQY. The manuscript was written by SC and improved by XQY, LS and JF. All authors reviewed and approved the final manuscript.

# References

1. An Z, Wu G, Li J, et al., 2015: Global Monsoon Dynamics and Climate Change. *Annu Rev Earth Pl Sc*, 43, 29–77.

2. Chang C, Lei Y, Sui C, et al., 2012: Tropical cyclone and extreme rainfall trends in East Asian summer monsoon since mid–20th century. *Geophys Res Lett*, 39.L18702, doi:10.1029/2012GL052945.

3. Chen H, Liu L, and Zhu Y, 2013: Possible linkage between winter extreme low temperature events over China and synoptic–scale transient wave activity. *Science China Earth Sciences*, 56, 1266–1280.

4. Ding Y, 1994: Monsoons over China. Atmospheric Sciences Library[M]. Holland: Kluwer Academy Publishers, pp419–420.

5. Ding Y, and Chan J, 2005: The East Asian summer monsoon: an overview. *Meteorol Atmos Phys*, 89, 117–142.

6. Dong L, Guo P, and Li X. 2006: Relationship between Activity of Transient Waves and Excessive/Deficit Summer Rain in Changjiang–Huaihe River Basin (in Chinese). *Journal of Nanjing Institute of Meteorology*, 29, 470–476.

7. Ding Y, Si D, Liu Y, et al., 2018: On the characteristics, driving forces and inter–decadal variability of the East Asian summer monsoon. *Chinese Journal of Atmospheric Sciences*, 42, 533–558.

8. Ding Y, Sun Y, Wang Z, et al., 2009: Inter–decadal variation of the summer precipitation in China and its association with decreasing Asian summer monsoon Part II: Possible causes. *Int J Climatol*, 29, 1926–1944.

9. Ding Y, Wang Z, and Sun Y, 2008: Inter–decadal variation of the summer precipitation in East China and its association with decreasing Asian summer monsoon. Part I: Observed evidences. *Int J Climatol*, 28, 1139–1161.

10. Enomoto T, Hoskins B, and Matsuda Y, 2003: The formation mechanism of the Bonin high in August. *Q J Roy Meteor Soc*, 129, 157–178.

11. Fang J, and Yang X, 2016: Structure and dynamics of decadal anomalies in the wintertime midlatitude North Pacific ocean–atmosphere system. *Clim Dynam*, 47, 1989–2007.

12. Halley E, 1686: An Historical Account of the Trade Winds, and Monsoons, Observable in the Seas between and Near the Tropicks, with an Attempt to Assign the Phisical Cause of the Said Winds. *Philosophical transactions (Royal Society (Great Britain) : 1683)*, 16, 153–168.

13. He J, Li J, and Zhu Q, 1989: Sensitivity experiments on summer monsoon circulation cell in East Asia. Adv Atmos Sci 6(1):120–132.

14. He J, Ju J, Wen Z, et al., 2007: A Review of Recent Advances in Research on Asian Monsoon in China. *Adv. Atmos. Sci.* 24, 972–992.

15. Holopainen E, Rontu L, and Lau N, 1982: The Effect of Large–Scale Transient Eddies on the Time–Mean Flow in the Atmosphere. *J Atmos Sci*, 39, 1972–1984.

16. Holton J,1979: An Introduction to Dynamic Meteorology, 2$^{nd}$ ed. *Academic Press*, 391pp.

17. Hoskins, B. J., 1983: Modeling of the transient eddies and their feedback on the mean flow. Large-Scale Dynamical Processes in the Atmosphere, B. J. Hoskins and R. Pearce, Eds., Academic Press, 169–199.

18. Huang R, Yong L, Du Z, et al., 2017: Differences and links between the East Asian and South Asian summer monsoon systems: Characteristics and Variability. *Adv Atmos Sci*, 34, 1204–1218.

19. Jin Q, Yang X, Sun X, et al., 2013: East Asian summer monsoon circulation structure controlled by feedback of condensational heating. *Clim Dynam*, 41, 1885–1897.

20. Kobayashi S, Ota Y, Harada Y, et al., 2015: The JRA-55 reanalysis: General specifications and basic characteristics. *J. Meteorol. Soc. Japan*, 93, 5–48, doi:10.2151/jmsj.2015-001.

21. Kosaka Y, Nakamura H, Watanabe M, et al., 2009: Analysis on the Dynamics of a Wave-like Teleconnection Pattern along the Summertime Asian Jet Based on a Reanalysis Dataset and Climate Model Simulations. *J Meteorol Soc Jpn*, 87, 561–580.

22. Lau K, 1992: East Asian summer Monsoon rainfall variability and climate teleconnection. *J Meteorol Soc Jpn*, 70, 211–242.

23. Lau K, Kim K, and Yang S, 2000: Dynamical and Boundary Forcing Characteristics of Regional Components of the Asian Summer Monsoon. *J Climate*, 13, 2461–2482.

24. Lau N, and Holopainen E, 1984: Transient eddy forcing of the time-mean flow as identified by geopotential tendencies. *J. Atmos. Sci.*, 41, 313–328, doi:10.1175/1520-0469(1984)041<0313:TEFOTT>2.0.CO;2.

25. Lau N, and Oort A, 1982: A Comparative Study of Observed Northern Hemisphere Circulation Statistics Based on GFDL and NMC Analyses. Part II: Transient Eddy Statistics and the Energy Cycle. *Mon. Weather Rev.*, 110, 889–906, doi:10.1175/1520-0493(1982)110<0889:ACSOON>2.0.CO;2.

26. Leung M, and Zhou W, 2015: Variation of circulation and East Asian climate associated with anomalous strength and displacement of the East Asian trough. *Clim Dynam*, 45, 2713–2732.

27. Li C, and Yanai M, 1996: The Onset and Interannual Variability of the Asian Summer Monsoon in Relation to Land-Sea Thermal Contrast. *J Climate*, 9, 358–375.

28. Li J, and Zeng Q, 2003: A new monsoon index and the geographical distribution of the global monsoons. *Adv Atmos Sci*, 20, 299–302.

29. Li M, and Luo Z, 1988: Effects of moist process on subtropical flow patterns and multiple equilibrium states. *Sci Sinica (B)*, 31, 1352–1361.

30. Li Z, Lau W, Ramanathan V, et al., 2016: Aerosol and monsoon climate interactions over Asia. *Rev Geophys*, 54, 866–929.

31. Li C and Yanai M.1996: Atmospheric circulation characteristics associated with the onset of Asian summer monsoon. *Adv Atmos Sci*, 23, 925–939.

32. Lindzen and Farrell. 1980: A simple approximate result for the maximum growth rate of baroclinic instabilities. *J Atmos Sci*, 37, 1648–1654

33. Liang X, Liu Y, and Wu G, 2006: Roles of tropical and subtropical land-sea distribution and the Qinghai-Xizang Plateau in the formation of the Asian summer monsoon. *Chin J Geophys* 49(4):983–

992 (in Chinese).

34. Liu Y, Chan J, Mao J, et al., 2002: The role of Bay of Bengal convection in the onset of the 1998 South China Sea summer monsoon. *Mon Weather Rev*, 130:2731−2744.

35. Liu Y, Wu G, Hong J, et al., 2012: Revisiting Asian monsoon formation and change associated with Tibetan Plateau forcing: II. Change. *Clim Dynam*, 39, 1183−1195.

36. Liu Y, Wu G, Liu H, et al., 2001: Condensation heating of the Asian summer monsoon and the subtropical anticyclone in the Eastern Hemisphere. *Clim Dynam*, 17, 327−338.

37. Luo D, 2005a: A barotropic envelope Rossby soliton model for block−eddy interaction. Part II: Role of westward−traveling planetary waves. *J Atmos Sci*, 62, 22−40.

38. Luo D, 2005b: A barotropic envelope Rossby soliton model for block−eddy interaction. Part III: Wavenumber conservation theorems for isolated blocks and deformed eddies. *J Atmos Sci*, 62, 3839−3859.

39. Luo D, Gong T, and Diao Y, 2007: Dynamics of eddy−driven low−frequency dipole modes. Part III: Meridional displacement of westerly jet anomalies during two phases of NAO. *J Atmos Sci*, 64, 3232−3248.

40. Luo H, and Yanai M, 1983: The large−scale circulation and heat sources over the Tibetan Plateau and surrounding areas during the early summer of 1979. Part I: precipitation and kinematic analyses. Mon Weather Rev 111:922−944.

41. Ma D, Boos W, and Kuang Z, 2014: Effects of Orography and Surface Heat Fluxes on the South Asian Summer Monsoon. *J Climate*, 27, 6647−6659.

42. Molnar P, Boos W, and Battisti D, 2010: Orographic Controls on Climate and Paleoclimate of Asia: Thermal and Mechanical Roles for the Tibetan Plateau. *Annu Rev Earth Pl Sc*, 38, 77−102.

43. Nakamura H, Izumi T, and Sampe T, 2002: Interannual and Decadal Modulations Recently Observed in the Pacific Storm Track Activity and East Asian Winter Monsoon. *J Climate*, 15, 1855−1874.

44. Park H, Lintner B, Boos W, et al., 2015: The Effect of Midlatitude Transient Eddies on Monsoonal Southerlies over Eastern China. *J Climate*, 28, 150904104833007.

45. Qi L, He J, Zhang Z, et al., 2008: Seasonal cycle of the zonal land−sea thermal contrast and East Asian subtropical monsoon circulation. *Chinese Science Bulletin*, 53, 131−136.

46. Qian W, and Jiang M. Early signals of synoptic−scale atmospheric anomalies associated with the summer low temperature events in Northeast China[J]. *Meteorology & Atmospheric Physics*, 2014, 124(1−2):33−46.

47. Qiu J, 2013: Monsoon Melee. *Science (American Association for the Advancement of Science)*, 340, 1400−1401.

48. Ramage C, 1971: Monsoon Meteorology [M]. New York: Academic Press.

49. Saha S, Moorthi S, Pan H, et al., 2010: The NCEP climate forecast system reanalysis. *Bulletin of The American Meteorological Society−Bull Amer Meteorol Soc*, 91. 1015−1057, doi:10.1175/2010BAMS3001.1.

50. Sang X , Yang X Q , Tao L , et al. Evaluation of Synoptic Eddy Activities and their Feedback onto the Midlatitude Jet in Five Atmospheric Reanalyses with Coarse Versus Fine Model Resolutions[J]. Climate Dynamics, 2021, 58(5-6):1363-1381.

51. Song F, and Zhou T, 2013: FGOALS-s2 Simulation of Upper-level Jet Streams over East Asia£ʃ Mean State Bias and Synoptic-scale Transient Eddy Activity. *Adv Atmos Sci*, 30, 739-753.

52. Sun X, Chen L, and He J, 2001: Interannual variation of index of East Asian land-sea thermal difference and its relation to monsoon circulation and rainfall over China. *Acta Meteorol. Sin.*, 15, 71-85.

53. Tan B. Advances of atmospheric of Rossby waves dynamics.2008: *Acta Meteorologica Sinica* (In Chinese), 66,  870⊠879.

54. Tao S, and Chen L, 1987: A Review of Recent Research on the East Asian Summer Monsoon in China[M]. Monsoon Meteorology.

55. Ting M, Wang H, and Yu L, 2001: Nonlinear stationary wave maintenance and seasonal cycle in the GFDL R30 GCM. *J Atmos Sci*, 58, 2331-2354.

56. Ueda H, and Yasunari T, 1998: Role of warming over the Tibetan Plateau in early onset of the summer monsoon over the Bay of Bengal and the South China Sea. J Meteorol Soc Jpn 76(1): 1-12.

57. Wang B, Ding Q, Fu X, et al., 2005: Fundamental challenge in simulation and prediction of summer monsoon rainfall. *Geophys Res Lett*, 15, 291-310.

58. Wang B, Ding Q, and Liu J. Concept of global monsoon[M]. The Global Monsoon System: Research and Forecast. 2011: 3-14.

59. Wang B, and Lin H, 2002: Rainy Season of the Asian-Pacific Summer Monsoon. *J Climate*, 15, 386-398.

60. Wang B, Lin H, Zhang Y, et al., 2004: Definition of South China Sea Monsoon Onset and Commencement of the East Asia Summer Monsoon. *Journal of Climate - J CLIMATE*, 17, 699-710.

61. Wang B, Liu J, Kim H, et al., 2012: Recent change of the global monsoon precipitation (1979-2008). *Clim Dynam*, 39, 1123-1135.

62. Webster P, Magaña V, Palmer T, et al., 1998: Monsoons: Processes, predictability, and the prospects for prediction. *J Geophys Res: Oceans, 103,* 14451-14510.

63. Webster P, and Yang S, 1992: Monsoon and Enso: Selectively Interactive Systems. *Q J Roy Meteor Soc*, 118, 877-926.

64. Wen M, He J, and Xiao Z, 2004: Impacts of the convection over the Indo-China Peninsula on the onset of SCS summer monsoon. Chin J Atmos Sci 28(6):864-875 (in Chinese).

65. Wu G, Duan A, Liu Y, et al., 2015a: Tibetan Plateau climate dynamics: recent research progress and outlook. *Natl Sci Rev*, 2, 100-116.6.

66. Wu G, and Liu H, 1998: Vertical vorticity development owing todown-sliding at slantwise isentropic surface. *Dyn Atmos Ocean,* 27:715-743.

67. Wu G, Liu Y, Dong B, et al., 2012b: Revisiting Asian monsoon formation and change associated with Tibetan Plateau forcing: I. Formation. *Clim Dynam*, 39, 1169-1181.

68. Wu G, Liu Y, He B, et al., 2012a: Thermal controls on the Asian summer monsoon. *Sci Rep-Uk*, 2, 404–404.

69. Wu G, Liu Y, He B, et al., 2018: Review of the Impact of the Tibetan Plateau Sensible Heat Driven Air-Pump on the Asian Summer Monsoon. *Chinese Journal of Atmospheric Sciences(In Chinese)*, 42, 488–504.

70. Wu G, Liu Y, Zhang Q, et al., 2007: The Influence of Mechanical and Thermal Forcing by the Tibetan Plateau on Asian Climate. *J Hydrometeorol*, 8, 770–789.

71. Wu G, Liu Y, and Liu P, 1999: The effect of spatially non-uniform heating on the formation and variation of subtropical high. Part I: scale analysis. *Acta Meteorol Sinica* 57(3):257–263 (in Chinese).

72. Wu G, and Zhang Y, 1998: Tibetan Plateau forcing and the timing of the monsoon onset over South Asia and the South China Sea. *Mon Weather Rev* 126:913–927.

73. Wu R, 2002: A mid-latitude Asian circulation pattern in boreal summer and its connection with the Indian and East Asian summer monsoons. *Int J Climatol*, 22, 1879 – 1895.

74. Xiang Y, and Yang X, 2012: The Effect of Transient Eddy on Interannual Meridional Displacement of Summer East Asian Subtropical Jet. *Adv Atmos Sci*, 29, 484–492.

75. Xie P, Chen M, Yang S, et al., 2007: A gauge-based analysis of daily precipitation over East Asia, *J. Hydrometeorol.*, 8, 607. 626.

76. Yanai M, and Wu G, 2006: Effects of the Tibetan Plateau. *Asian Monsoon*, 29, 513–549.

77. Ye D, 1981: Some characteristics of the summer circulation over the Qinghai-Xizang (Tibet) Plateau and its neighborhood. *Bull Am Meteorol Soc* 62:14–19.

78. Ye D, and Wu G, 1998: The role of the heat source of the Tibetan Plateau in the general circulation. *Meteorol Atmos Phys* 67:181–198.

79. Yeh T, 1957: The wind structure and heat balance in the lower troposphere over Tibetan Plateau and its surroundings. *Acta Meteorol. Sin.*, 28, 505–506.

80. Yeh T, 1982: Some aspects of the thermal influences of the Qinghai Tibetan Plateau on the atmospheric circulation. *Arch Meteorol Geophys Bioklim* 31A:205–220.

81. Zhang Q, and Tao S,1998: Influence of Asian mid-high latitude circulation on East Asian summer rainfall. *Acta Meteorol Sinica* 56: 199–211 (in Chinese).

82. Zhang Y, Stone P, and Solomon A, 2009: The Role of Boundary Layer Processes in Limiting PV Homogenization. *J Atmos Sci*, 66, 1612–1632.

83. Zhao L, and Wang J, 2014: Robust Response of the East Asian Monsoon Rainband to Solar Variability. *J Climate*, 27, 3043–3051.

84. Zhou T, Wu B, Guo Z, et al., 2018: A review of East Asian summer monsoon simulation and projection: Achievements and problems, opportunities and challenges. *Chinese Journal of Atmospheric Sciences (in Chinese)*, 4, 902–934.

85. Zhu K, 1934: The Enigma of Southeast Monsoon in China. *J. Geographical Society of China (in Chinese)*, 1, 1–27.

86. Zhu Q, He J, and Wang P, 1986: A study of circulation differences between East–Asian and Indian summer monsoons with their interaction. *Adv Atmos Sci*, 3, 466–477.
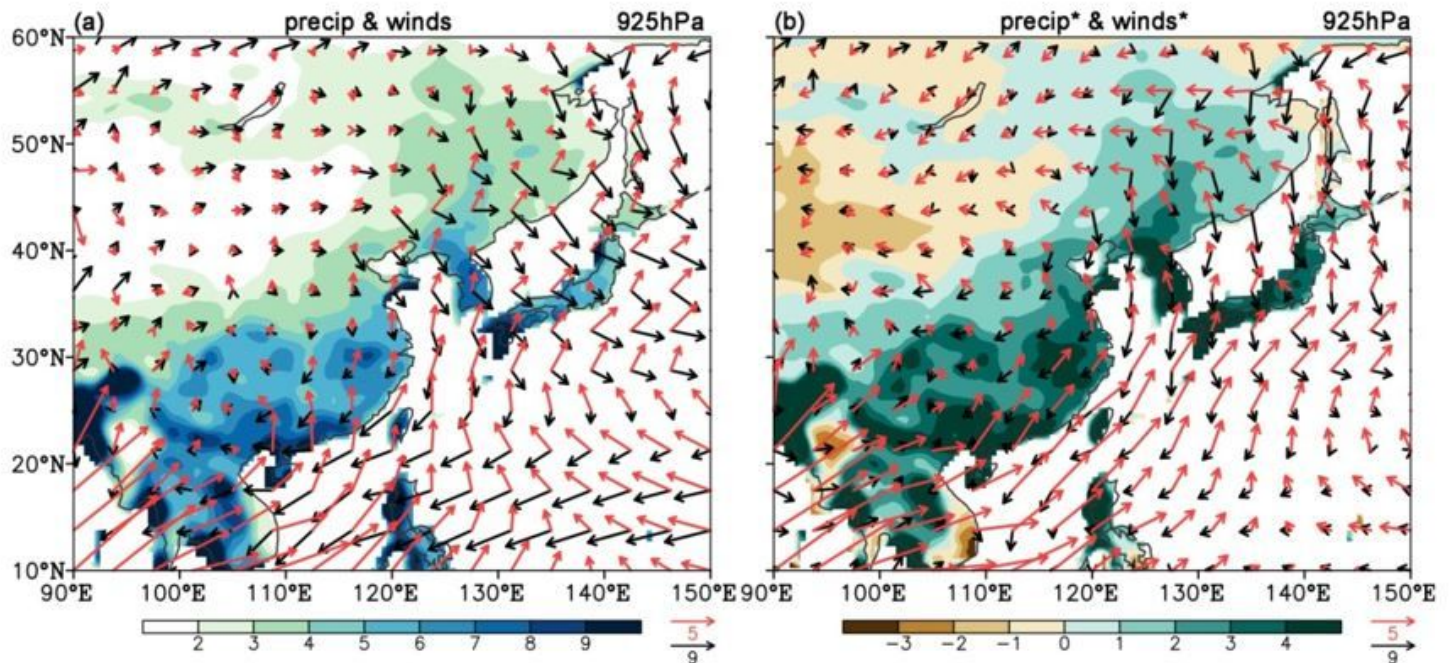
# Figures



Figure 1

(a) Climatological summertime precipitation rate (shaded, mm·day$^{-1}$) and 925 hPa winds (vectors, m·s$^{-1}$) for the period of 1980–2019. (b) as in (a), but for the corresponding deviations obtained by subtracting the globally zonal mean. Red (black) vectors denote the winds in boreal summer (winter).
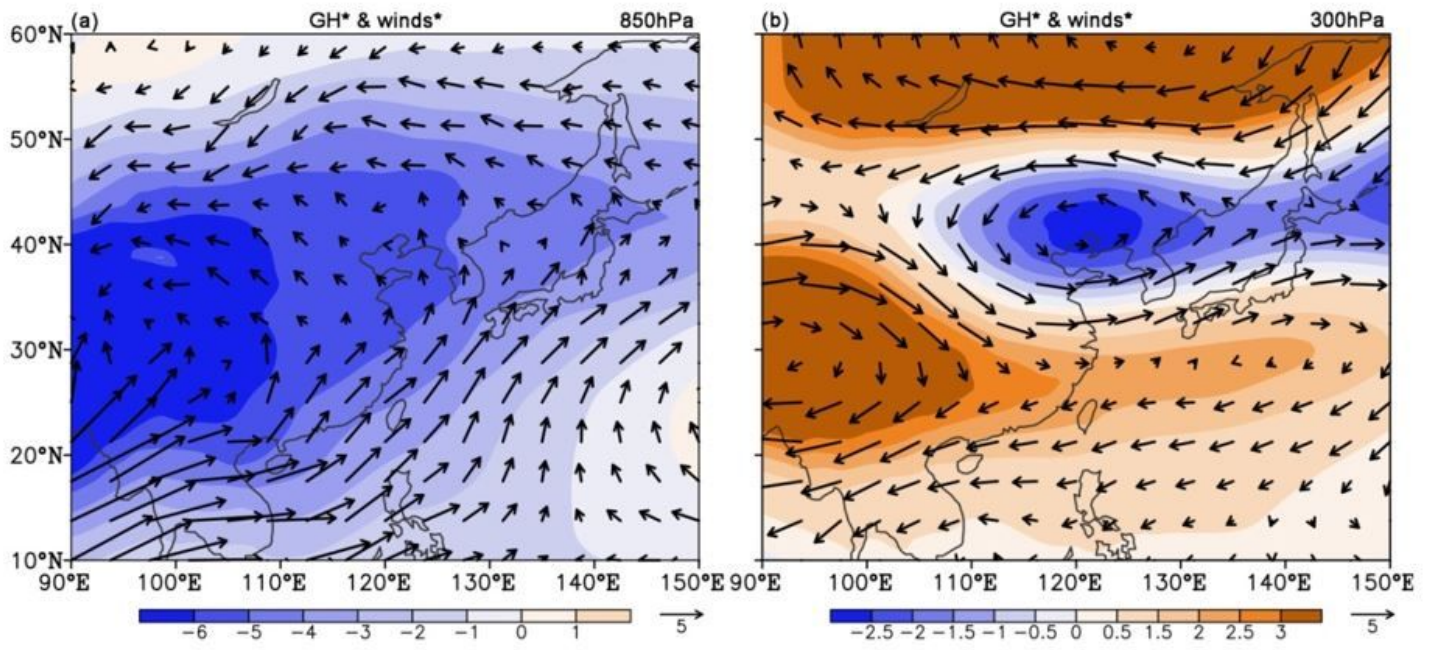
**Figure 2**

The deviations of climatological geopotential heights (shaded, dagpm) and winds (vectors, m·s$^{-1}$) at 850hPa (a) and 300 hPa (b) in summer for the period of 1980−2019. The deviations are obtained by subtracting the globally zonal mean.
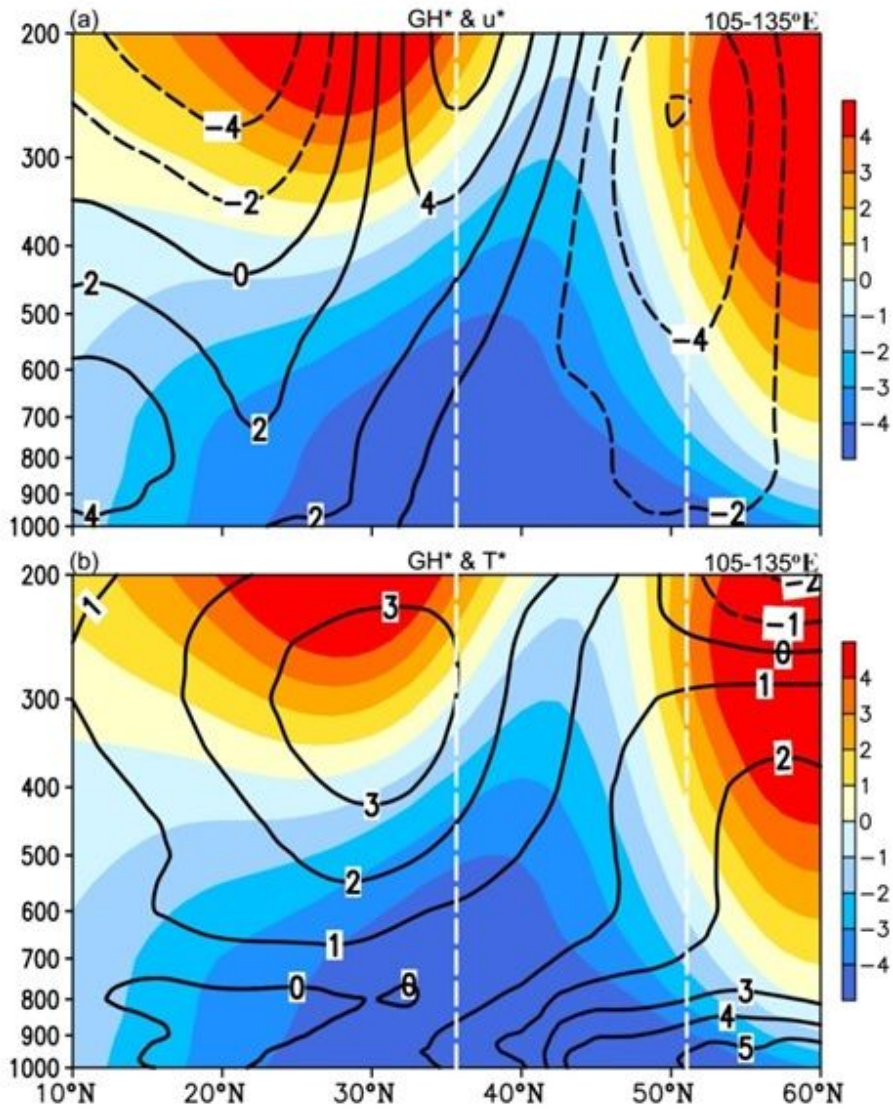
**Figure 3**

(a) Latitude–altitude sections averaged within 105–135ºE of the deviations of climatological geopotential height (shaded, dagpm) and zonal winds (contours, m·s$^{-1}$) in summer for the period of 1980–2019. (b) as in (a), but for geopotential height (shaded, dagpm) and temperature (contours, K). The deviations are obtained by subtracting the globally zonal mean. The white dashed lines denote the latitudes of 35.5ºN and 50.5ºN, respectively.
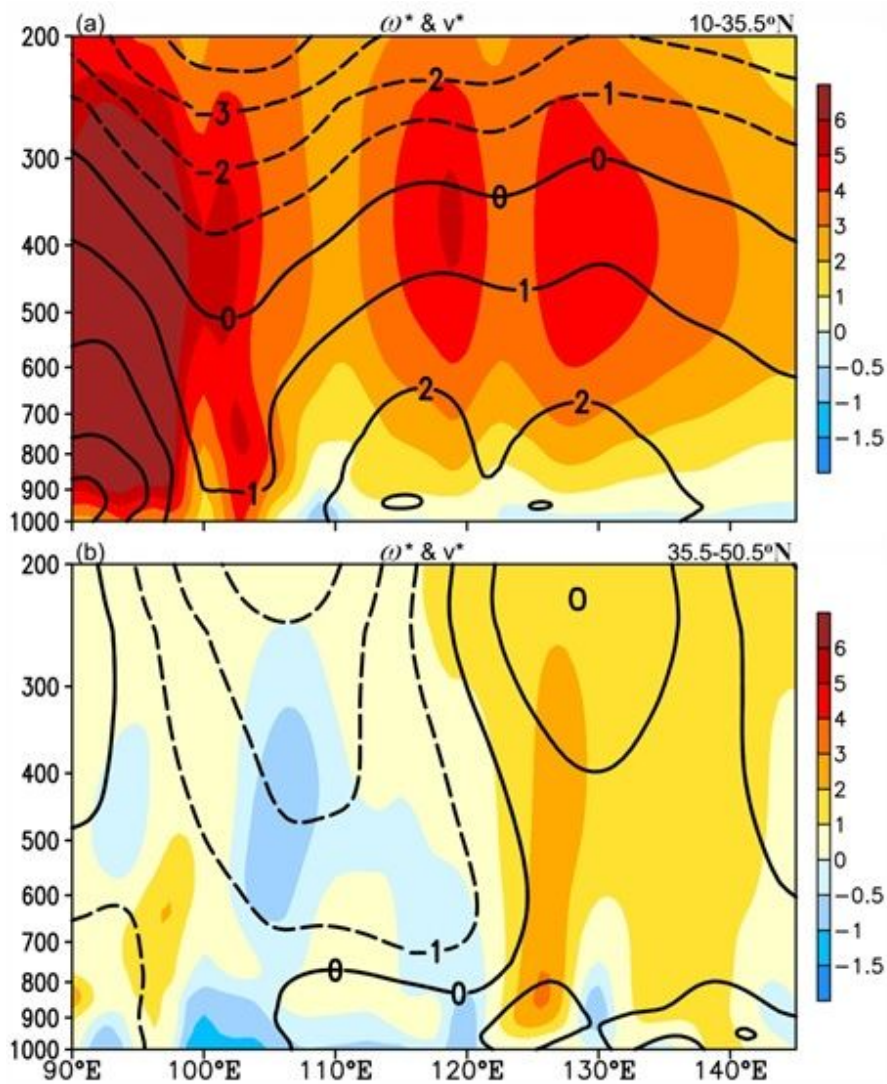
**Figure 4**

Latitude−altitude sections of the deviations of climatological vertical velocity (shaded, $-1\times10^{-2}\,\mathrm{Pa\cdot s^{-1}}$) and meridional wind (contours, $\mathrm{m\cdot s^{-1}}$) averaged within $10\degree-35.5\degree N$ (a) and $35.5\degree-50.5\degree N$ (b) in summer for the period of 1980−2019. The deviations are obtained by subtracting the globally zonal mean.
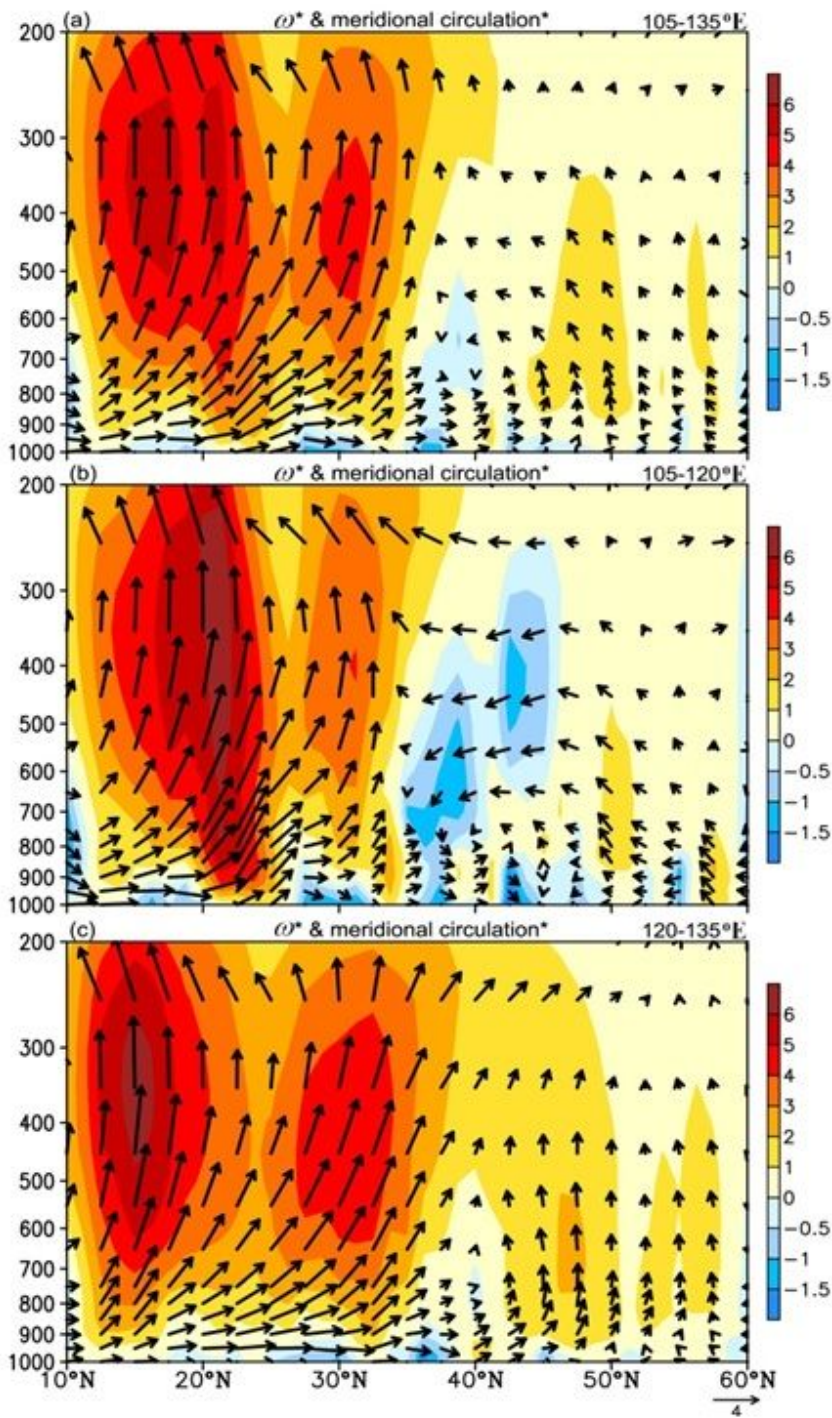
## Figure 5

Latitude−altitude sections of the deviations of climatological meridional circulation (vectors, m·s$^{-1}$) and vertical velocity (shaded, $-1\times10^{-2}$Pa·s$^{-1}$) averaged within 105°−135°E (a), 105°−120°E (b) and 120°−135°E (c) in summer for the period of 1980−2019. The deviations are obtained by subtracting the globally zonal mean.
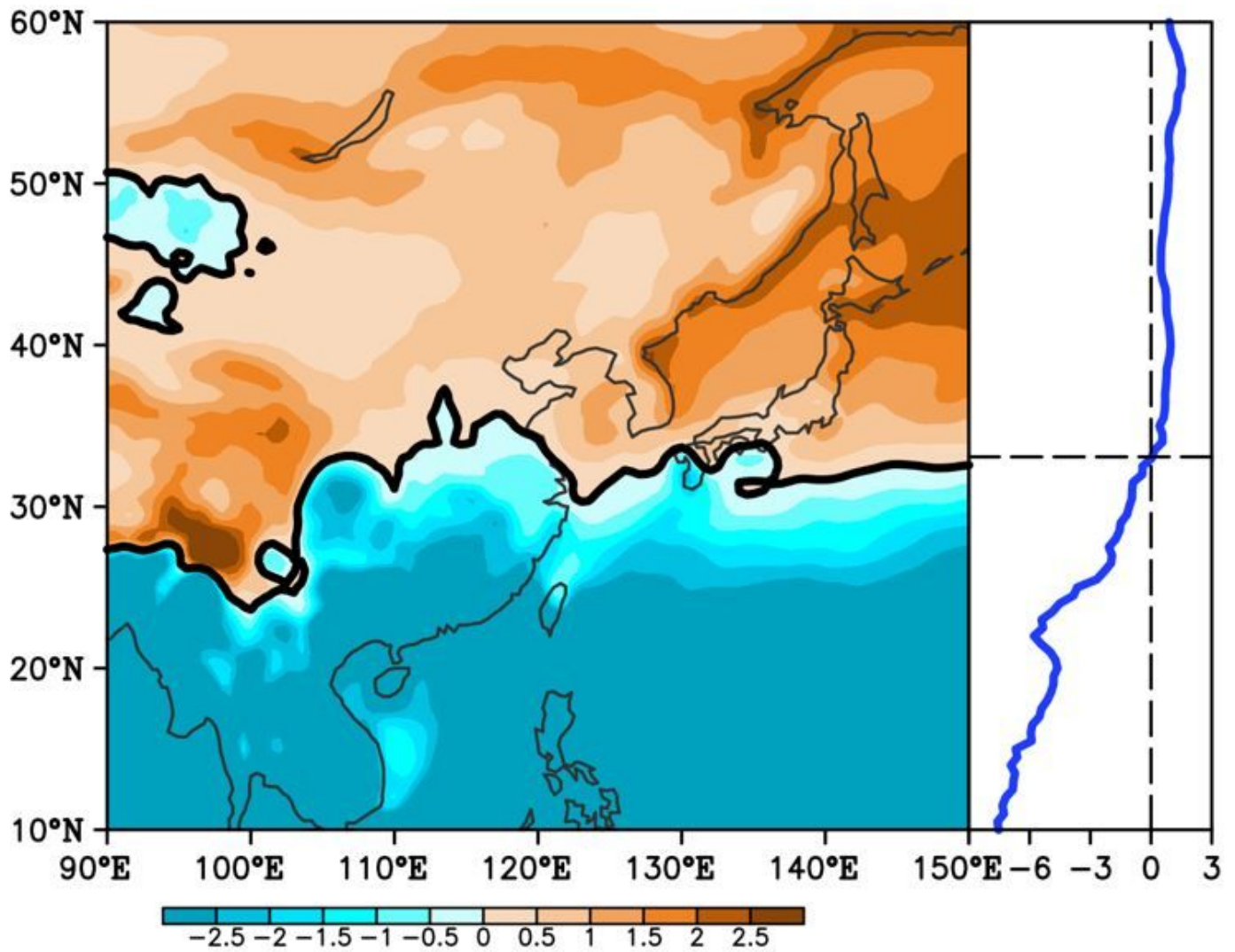
**Figure 6**

Horizontal distribution (left panel) and the profile with latitudes within 105°−135°E (right panel) of the difference value between the large scale and convective precipitation rate (shaded, mm·day$^{-1}$) based on the CSFR reanalysis data.
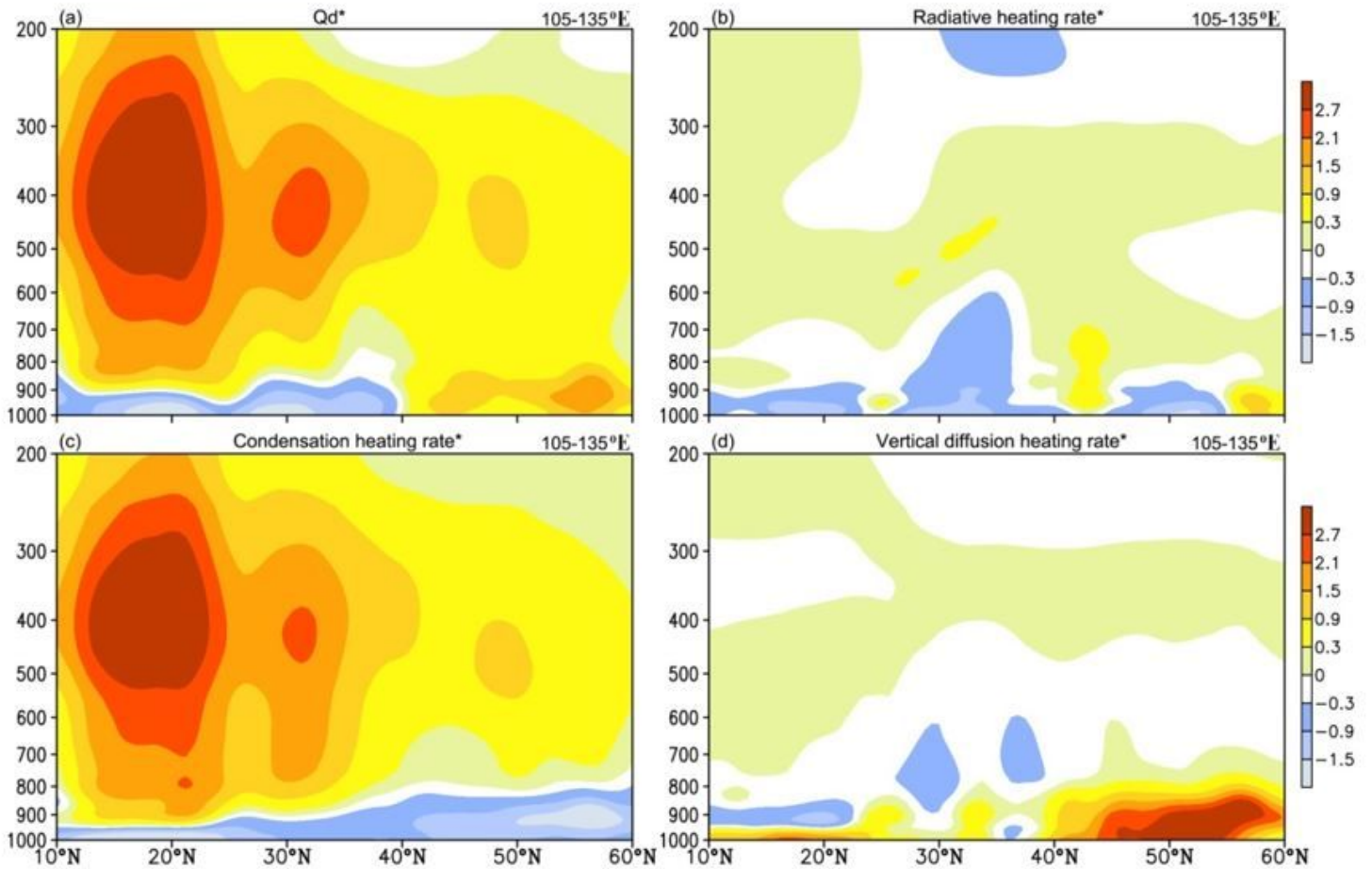
**Figure 7**

Longitude−altitude sections of the deviations of climatological diabatic heating rate (a), radiative heating rate (b), condensation heating rate (c) and vertical diffusion heating rate (f) averaged within 105º−135ºE in summer for the period of 1980−2019. The deviations are obtained by subtracting the globally zonal mean, and the unit is K·day$^{-1}$.
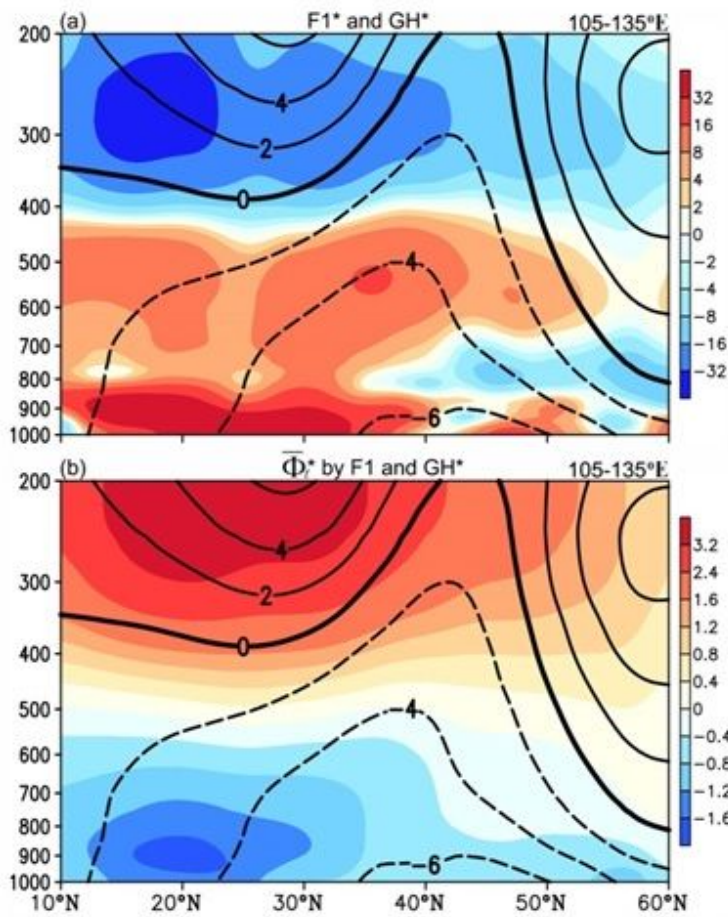
**Figure 8**

Longitude−altitude sections of the deviations of climatological diabatic heating forcing term ($F_1$) (a, shaded, $10^{-11}$ s$^{-2}$) and the geopotential tendencies induced by the diabatic heating forcing (b, shaded, $10^{-3}$ m$^2$·s$^{-3}$) averaged within 105−135°E in summer for the period 1980−2019. The geopotential height deviations are presented in contours in the (a) and (b). Contours represent the deviations of climatological geopotential height. The deviations are obtained by subtracting the globally zonal mean.
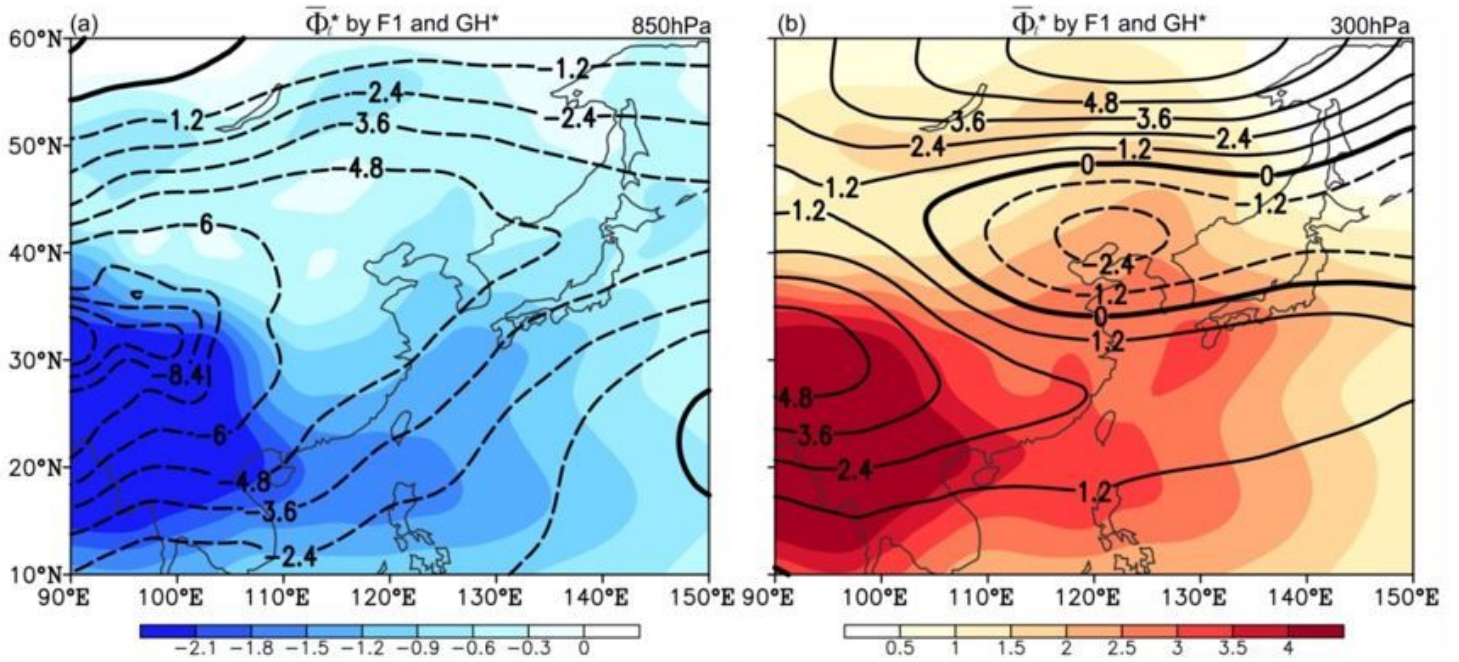
**Figure 9**

Horizontal distribution of the deviations of climatological geopotential tendencies induced by the diabatic heating forcing term ($F_1$) (shaded, $10^{-3}$ m²·s⁻³) and the climatological geopotential height (contours, dagpm) respectively at 850hPa (a) and 300 hPa (b) in summer for the period of 1980–2019. The deviations are obtained by subtracting the globally zonal mean.
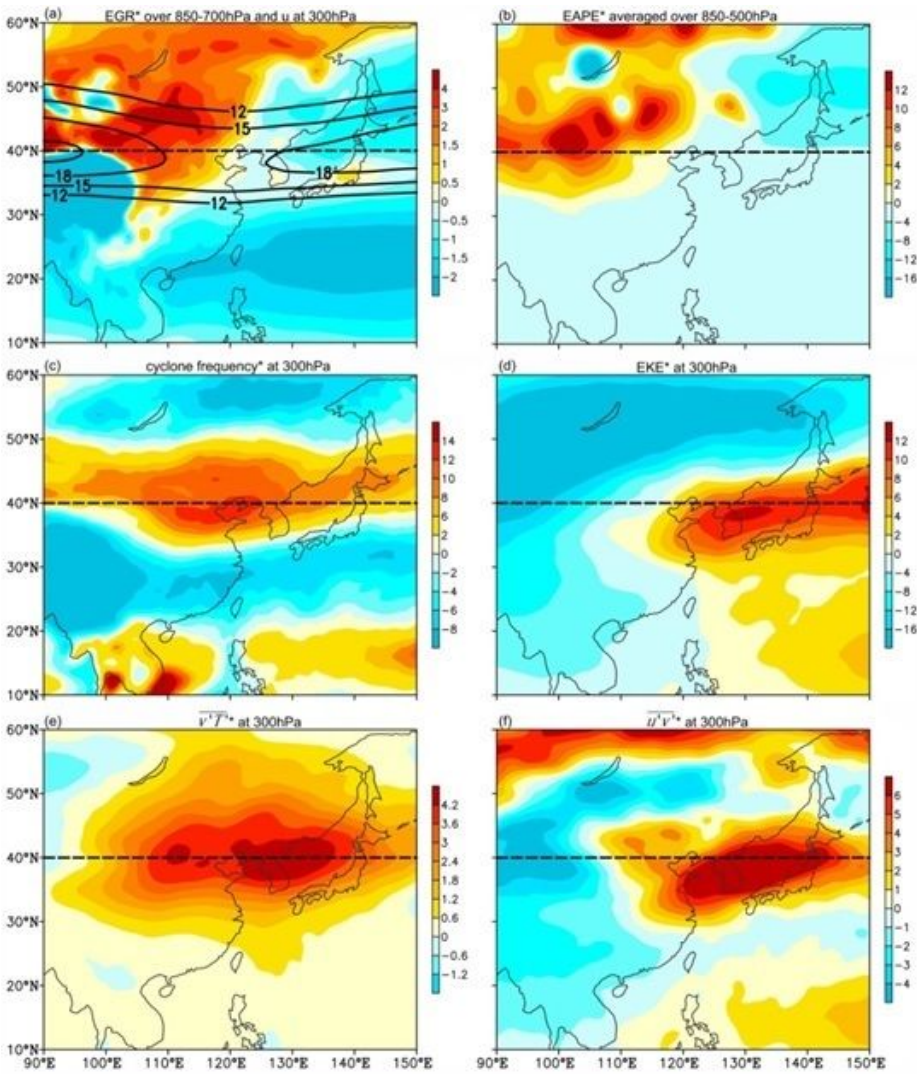
The deviations of climatological maximum Eady growth rate (EGR) between 850 and 700 hPa (a, day$^{-1}$), the eddy available potential energy (EAPE) averaged over the 850–500 hPa (b, $m^2 \cdot s^{-2}$), the cyclone frequency (c), the eddy kinetic energy (EKE) (d, $m^2 \cdot s^{-2}$), the eddy heat flux $\overline{v'T'}$ (e, $K \cdot m \cdot s^{-1}$) and the eddy momentum flux $\overline{u'v'}$ (f, $m^2 \cdot s^{-2}$) at 300hPa in summer for the period 1980–2019. The contours with internals of $3\,m \cdot s^{-1}$ in (a) are the zonal wind exceeding $12\,m \cdot s^{-1}$ at 300hPa. The dashed line denotes the latitude of 40°N. The deviations are obtained by subtracting the globally zonal mean.

Figure 10

See image above for figure legend
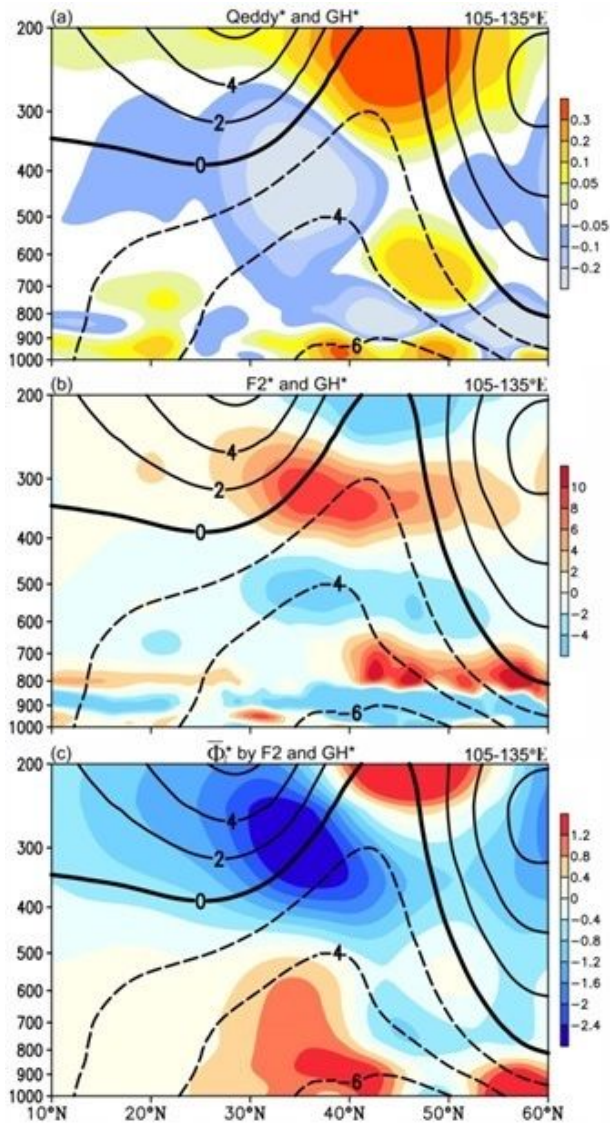
Longitude–altitude sections of the deviations of climatological transient eddy heating forcing $\overline{Q}_{eddy}$ (a, shaded, K·day$^{-1}$), the transient eddy heating forcing term ($F_2$) (b, shaded, $10^{-11}$ s$^{-2}$) and the geopotential tendencies induced by transient eddy heating forcing (c, shaded, $10^{-4}$ m$^2$·s$^{-3}$) averaged within 105°–135°E in summer for the period of 1980–2019. The geopotential height deviations are presented in contours in the (a) –(c). The deviations are obtained by subtracting the globally zonal mean.

Figure 11

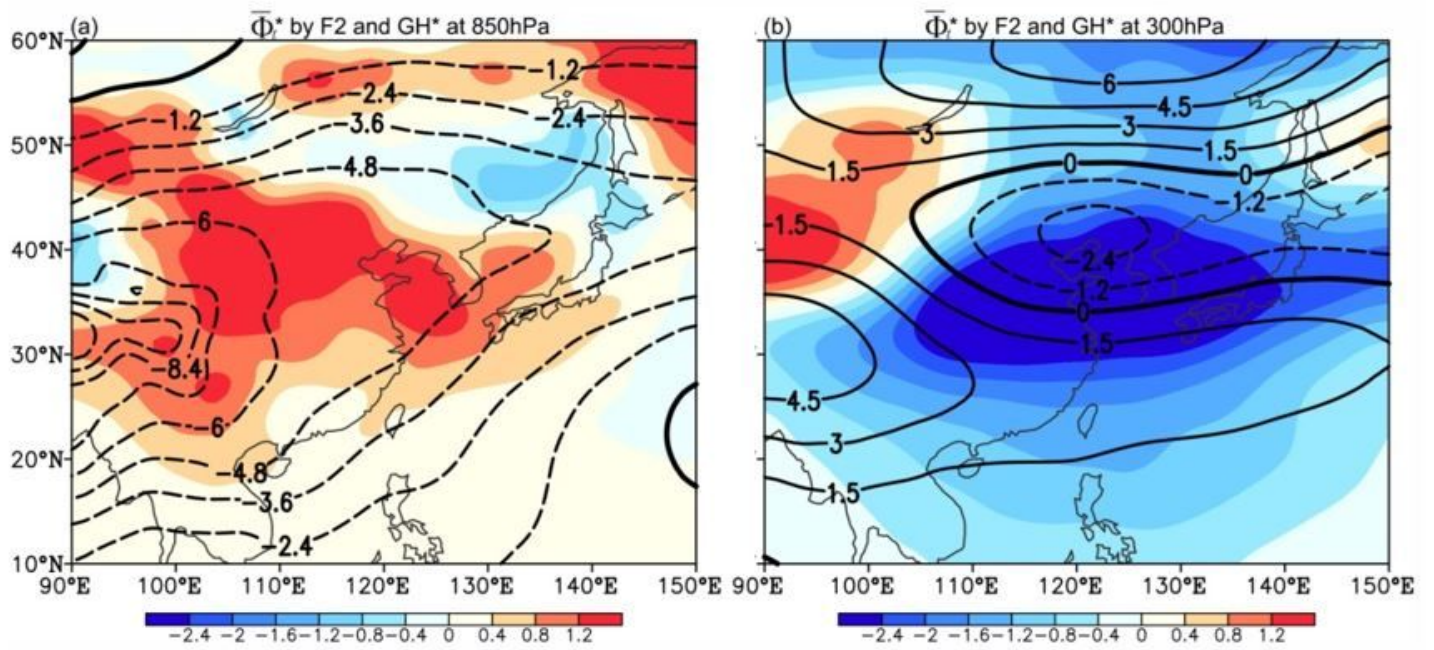See image above for figure legend

**Figure 12**

Horizontal distribution of the deviations of climatological geopotential tendencies induced by ($F_2$) (shaded, $10^{-4}$ m$^2$·s$^{-3}$) and the observed geopotential height (contours, dagpm) at 850 hPa (a) and 300 hPa (b) in summer for the period of 1980−2019. The deviations are obtained by subtracting the globally zonal mean.
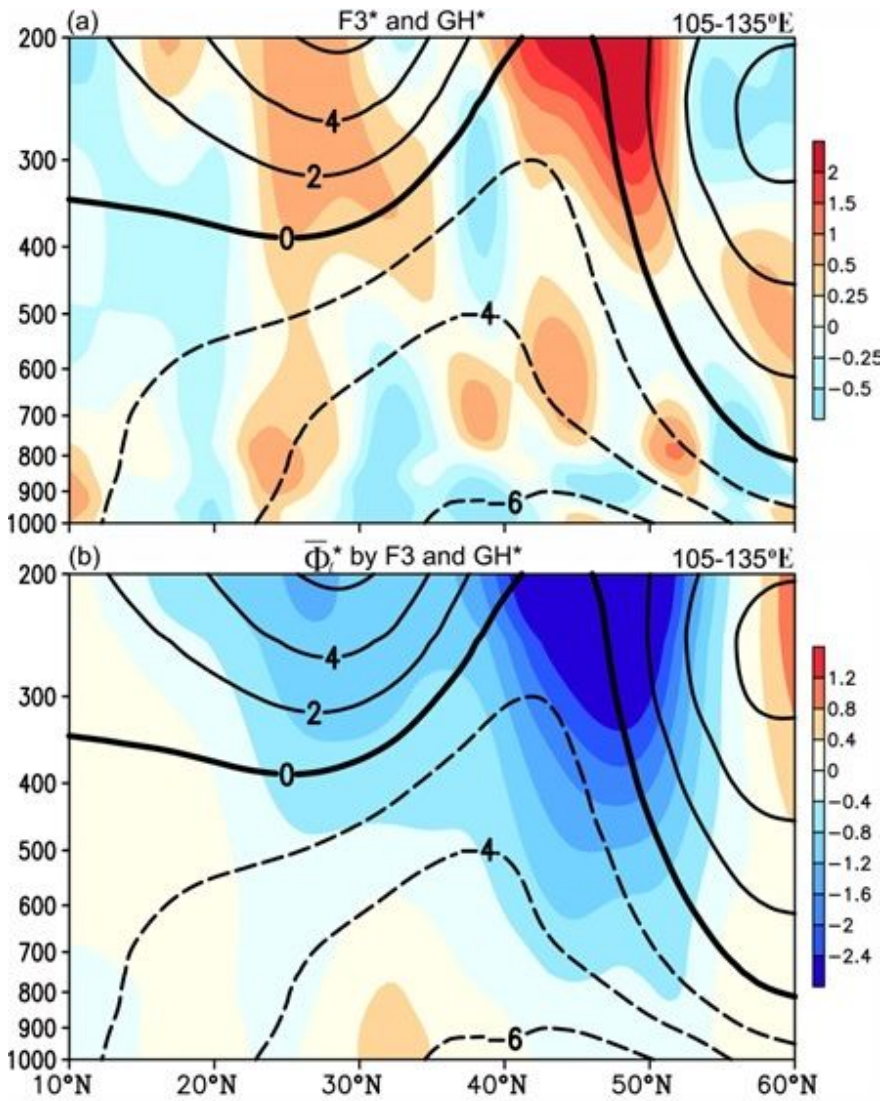
**Figure 13**

Longitude−altitude sections of the deviations of climatological transient eddy voriticity forcing term ($F_3$) (a, shaded, $10^{-11}$ $s^{-2}$) and the associated geopotential tendencies (b, shaded, $10^{-4}$ $m^2 \cdot s^{-3}$) induced by the transient eddy voriticity forcing averaged within 105°−135°E in summer for the period 1980−2019. The geopotential height deviations are presented in black contours in the (a) and (b). The deviations are obtained by subtracting the globally zonal mean.
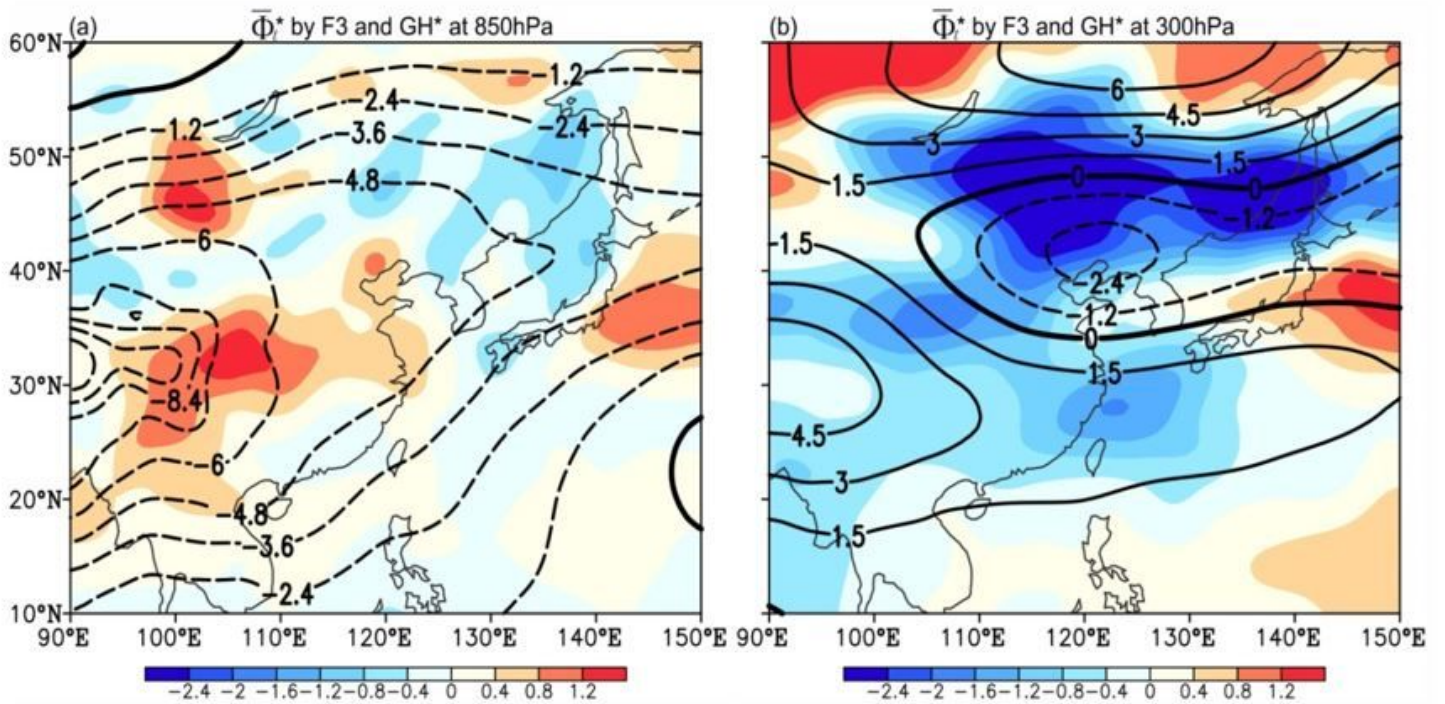
**Figure 14**

Horizontal distribution of the deviations of climatological geopotential tendencies induced by the transient eddy voriticity forcing (shaded, $10^{-4}$ $m^2 \cdot s^{-3}$) and the observed geopotential height (contours, dagpm) at 850 hPa (a) and 300 hPa (b) in summer for the period of 1980−2019. The geopotential height deviations are presented in contours in the (a) and (b). The deviations are obtained by subtracting the globally zonal mean.
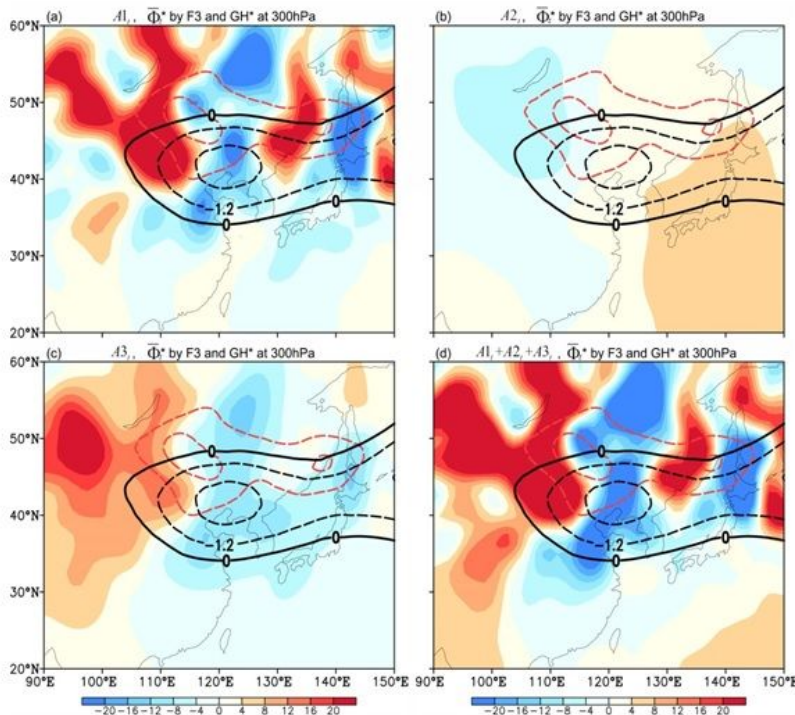
The horizontal distribution of the three types of advection effects that adjust the initial atmospheric response to the transient eddy vorticity forcing at 300 hPa in summer for the period of 1980–2019. (a) the relative vorticity produced by the transient eddy vorticity forcing advected by the globally zonal mean flow ( $-\dfrac{U}{f}\dfrac{\partial \nabla^2 \overline{\Phi}_{t,\overline{F}eddy}}{\partial x}$ ) (shaded, $10^{-16}$ s$^{-3}$). (b) the ambient vorticity advected by the induced meridional flows by the transient eddy vorticity forcing ( $-\dfrac{\beta}{f}\dfrac{\partial \overline{\Phi}_{t,\overline{F}eddy}}{\partial x}$ ) (shaded, $10^{-16}$ s$^{-3}$). (c) the stretching vorticity produced by the transient eddy vorticity forcing advected by the globally zonal mean flow ( $-U\dfrac{\partial}{\partial x}[\dfrac{\partial}{\partial p}(\dfrac{f}{\sigma_1}\dfrac{\partial \overline{\Phi}_{t,\overline{F}eddy}}{\partial p})]$ ) (shaded, $10^{-16}$ s$^{-3}$). (d) is the accumulation of the three types of advection effects (shaded; $10^{-16}$ s$^{-3}$). The observed geopotential height deviations less than 0 dagpm is presented in black in the intervals of 1.2 dagpm. The deviations of geopotential tendencies by the transient eddy vorticity forcing less than $-2\times10^{-4}$ m$^2$·s$^{-3}$ is presented in red contours in the intervals of $1\times10^{-4}$ m$^2$·s$^{-3}$. The deviations are obtained by subtracting the globally zonal mean.

Figure 15

See image above for figure legend